

Scalable high-resolution forecasting of sparse spatiotemporal events with kernel methods: a winning solution to the NIJ “Real-Time Crime Forecasting Challenge”

Seth Flaxman¹, Michael Chirico², Pau Pereira³, and Charles Loeffler⁴

¹Department of Mathematics and Data Science Institute, Imperial College London

²Grab, Singapore

³Amazon, Inc.

⁴Department of Criminology, University of Pennsylvania

June 28, 2022

Abstract

We propose a generic spatiotemporal event forecasting method, which we developed for the National Institute of Justice’s (NIJ) Real-Time Crime Forecasting Challenge [NIJ, 2017]. The goal of the competition was to predict several different types of crime hotspots over varying horizons for Portland, Oregon using calls-for-service data from the Portland Police Bureau (PPB). Our solution to the challenge is a spatiotemporal forecasting model combining scalable randomized Reproducing Kernel Hilbert Space (RKHS) methods for approximating Gaussian processes with autoregressive smoothing kernels in a regularized supervised learning framework. While the smoothing kernels capture the two main approaches in current use in the field of crime forecasting, heatmap-based (kernel density estimation) and the self-exciting point process (SEPP) models, the RKHS component of the model can be understood as an approximation to the popular log-Gaussian Cox Process model. For inference, we discretize the spatiotemporal point pattern and learn a log intensity function using the Poisson likelihood and highly efficient gradient-based optimization methods. Model hyperparameters including quality of RKHS approximation, spatial and temporal kernel lengthscales, number of autoregressive lags, bandwidths for smoothing kernels, as well as cell shape, size, and rotation, were learned using temporal crossvalidation. Resulting predictions significantly exceeded baseline KDE estimates; we had winning submissions to the competition in each of the different crime types, suggesting that our method is generically applicable. Performance improvement over baseline predictions and competing submissions were particularly large for sparse crimes over short forecasting horizons.

1 Introduction

The goal of the NIJ Real-Time Crime Forecasting Competition was to accurately forecast hotspots for several categories of calls-for-service to the Portland Police Bureau (PPB) in Portland, Oregon. Contestants submitted forecasts on (or before) February 28, 2017 for various time horizons starting on March 1, 2017 and extending as late as May 31, 2017. The hotspot predictions were scored based on two non-standard metrics related to their accuracy. Contest rules required that contestants predict which of the 62,500 - 360,000 square foot cells¹ within PPB’s 147.71 square mile service area would have the highest density of calls-for-service, with the total forecast area being no smaller than 0.25 square miles and no larger than 0.75 square miles, equivalent to forecasting 175–525 city blocks out of a total of 103,397 blocks². Prizes were given out for five different cumulative forecast periods (1 week, 2 weeks, 4 weeks, 8 weeks, 12 weeks), four different crime categories (Burglary, Street Crimes, Theft of Autos, All Calls for Service), and two different accuracy metrics.

While the specifics of the competition introduced peculiarities into the proposed solution, the basic structure of the problem is one of spatiotemporal forecasting of crime. This topic has been the focus of considerable attention in recent years as academic researchers, municipal police departments, and commercial entities have all sought to build forecasting tools that use police data to predict when and where both common and rare crimes are most likely to occur [Perry et al., 2013]. The earliest crime forecasting tools consisted of nothing more than pin-maps, with an example shown in Figure 1. Subsequent tools have adopted a range of different smoothing techniques to augment this method [Levine, 2004, Gorr et al., 2003, Gorr and Lee, 2015, Chainey et al., 2008b, Johnson et al., 2009].³

Similarly to other spatiotemporal forecasting applications (e.g., insurgent attacks, disease outbreaks, environmental hazards) [Lewis et al., 2011, Zammit-Mangion et al., 2012], forecasting crime leverages the structure of historical reported event information to identify areas of elevated risk in the future. Unlike these other spatiotemporal forecasting problems, forecasting crime involves an unusually heterogeneous set of events ranging from frequent and clustered events such as retail thefts and common assaults to much sparser incidents such as sexual assaults and burglaries.

To solve this problem, a range of forecasting methods have been proposed and demonstrated [Perry et al., 2013]. Many are model-driven, based on theories of crime causation [Caplan et al., 2011, Mohler et al., 2011]. Some use additional information, such as weather, demographics, and even social media [Wang et al., 2012]. Most rely on nothing more than past events to forecast future events [Chainey et al., 2008a, Kang and Kang, 2017], which suggests that spatiotemporal methods that are effective at forecasting crime could readily be generalized to an increasing number of real-time spatiotemporal forecasting problems [Taddy, 2010]. Possible applications for real-time forecasting methods include transportation demand models, computer network load

¹The extremes correspond to 250 ft by 250 ft and 600 ft by 600 ft squares, respectively; NIJ also introduced a minimum dimension of 125 feet [NIJ, 2017].

²Portland city blocks are small compared to other American cities at 200 feet on a side; see <https://www.strongtowns.org/journal/2013/11/27/optimizing-the-street-grid.html>

³Note that forecasting crime in general and forecasting crimes reported to the police in particular are often conflated, yet some types of crimes are systematically underreported, and simultaneously police focus their efforts on some classes of crimes and not others, e.g. street crime vs. white collar crime. For a compelling artistic representation of this issue, see the New Inquiry’s “White Collar Crime Risk Zones,” <https://whitecollar.thenewinquiry.com/> [Lavigne et al., 2017].



Figure 1: Early use of crime pin-maps at Scotland Yard.

models, wind turbine net capacity factor forecasting, and energy utilization patterns. At the same time, most methods and models currently used for spatiotemporal forecasting, including crime forecasting, were originally developed to answer inferential questions and have been adapted for use in forecasting [Breiman et al., 2001, Shmueli et al., 2010]. This often means that key model parameters are incompletely optimized for forecasting accuracy.

We make the following contributions: we propose a flexible, generic, and scalable spatiotemporal forecasting model, casting the problem of spatiotemporal forecasting explicitly as a supervised learning problem, while incorporating existing and highly successful modeling approaches from the spatiotemporal statistics literature. Our supervised learning setup gives us a coherent framework for the time-consuming task of optimizing hyperparameters, while our scalable approach to modeling and inference ensures that the model parameters themselves can be learned quickly enough to enable real-time forecasting. Our approach achieves accuracy improvements well beyond those generated by existing best-practices in crime prediction [Chainey et al., 2008a, Johnson et al., 2009].

The rest of this paper is laid out as follows. Section 2 describes the use of Gaussian processes for spatiotemporal learning and its application to the motivating problem. Section 3 reviews prior related work on spatiotemporal forecasting and spatiotemporal crime forecasting. Section 4 describes our model. Section 5 describes the details of the NIJ forecasting competition. Section 6 reports the results of the modeling exercise. Section 7 concludes with a discussion of implications for future work on spatiotemporal prediction of crime and related phenomenon.

2 Gaussian processes for spatiotemporal learning

2.1 Spatial statistics

The fundamental problem of spatiotemporal statistics is that, unlike in classical statistics, we cannot assume that observations in a dataset are either independent or identically distributed (iid). In the language of Tobler’s First Law of Geography [Tobler, 1970], “everything is related to everything else.” In the case of time series, a variety of successful approaches are available to deal with this issue: transformation of data in various ways such as differencing so that it is (approximately) iid, or employment of autoregressive (AR) and other classes of standard models. Similarly, spatial statistics features well-developed methods like kriging and models like the Conditional Autoregressive (CAR) model. However, the nascent field of spatiotemporal statistics—which has emerged alongside ever larger and richer datasets—does not yet feature widely applicable methods or models. Following Cressie and Wikle [2011] and much of the spatial statistics literature, we use Gaussian processes as the fundamental modeling approach for spatiotemporal data. In the particular case of point pattern data such as crime events, we follow Diggle et al. [2013] in considering the log-Gaussian Cox Process.

A Gaussian process is a stochastic model which can be used as a nonparametric prior over functions f . See Rasmussen and Williams [2006] for a comprehensive introduction. f is defined on some index set \mathcal{X} and for our purposes we will assume that f is real-valued, so $f : \mathcal{X} \rightarrow \mathcal{R}$. f is parameterized by a mean function μ and a covariance kernel function $k(\cdot, \cdot)$:

$$f \sim \mathcal{GP}(\mu, k(\cdot, \cdot)) \tag{1}$$

meaning that:

$$E[f(x)] = \mu(x) \tag{2}$$

$$\text{Cov}(f(x), f(x')) = k(x, x') \tag{3}$$

The defining feature of a Gaussian process is that at any finite set of indices $x_1, \dots, x_n \in \mathcal{X}$, the distribution of the vector $[f(x_1), \dots, f(x_n)]^\top$ is a multivariate Gaussian:

$$[f(x_1), \dots, f(x_n)]^\top \sim \mathcal{MVN}([\mu(x_1), \dots, \mu(x_n)]^\top, K) \tag{4}$$

where the covariance matrix $K_{ij} = k(x_i, x_j)$.

Gaussian processes are often described as a nonparametric model, since the number of parameters grows with the sample size, with attractive posterior consistency results in a simple regression setting [Choi and Schervish, 2007], and more intriguingly for our setup below when used as part of a Cox survival model [Fernandez and Teh, 2016]. While these theoretical results are comforting, our setting is fundamentally one of limited data (e.g. reported burglaries are rare, thankfully!) We thus focus more than might be typical in the literature on the parametric aspects of the Gaussian process model, that is, the mean function μ and the covariance kernel $k(\cdot, \cdot)$. Below, we discuss how these have been hand-crafted, based on prior knowledge and

to aid in interpretability.

2.2 Our previous work

Our model is based on the crime forecasting model developed by Flaxman [2014]. Inspired by small area disease mapping, this model handles a point pattern of Chicago crime data by aggregating it into 77 community areas (neighborhoods) by week and uses a Gaussian process to model the log-rate of crimes with a Poisson observation model:

$$\log n_{st} \sim \text{Poisson}(\exp(f) \cdot e_s) \quad (5)$$

$$f \sim \mathcal{GP}(0, k(\cdot, \cdot)) \quad (6)$$

with e_s giving the expected count (estimated from historical data) at location s . As described by Flaxman [2014, Section 3], the covariance kernel is the sum of a purely spatial kernel, a purely temporal kernel, a separable product of space and time kernels, and a periodic temporal kernel with period 52, designed to capture weekly cycles in the data. This additive structure combines the benefits of nonparametric methods with the interpretability of additive methods, as each of the separate kernels can pick up a different trend in the data, allowing these trends to be decomposed and their relative contributions assessed. This is visualized in Fig. 2 from Flaxman [2014].

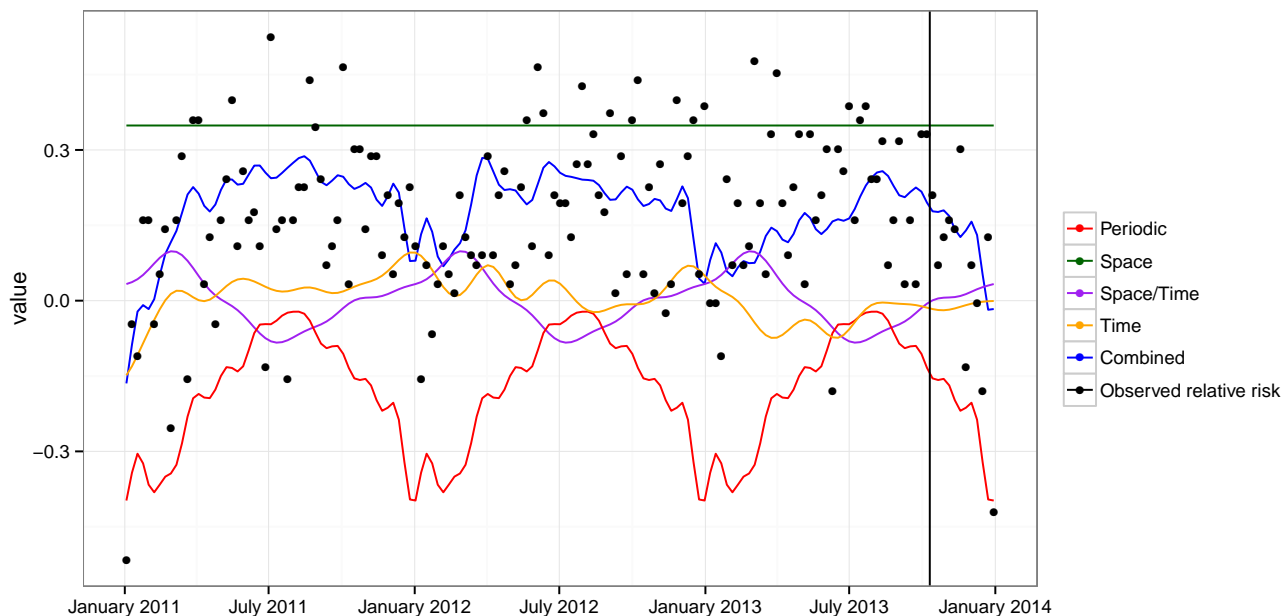


Figure 2: Predictions for a neighborhood in Chicago decomposed into additive components (periodic in time, space, space/time, and time) on the log-relative risk scale. Since the predictions are shown over time, the spatial component does not vary, but other neighborhoods had different space and space/time trends.

Building on this model, Flaxman et al. [2015] propose that instead of specifying an additive kernel structure, it is possible to learn it directly from the data, given enough data and a rich enough class of kernels. But this assumes that it is possible to perform inference with very large datasets as the standard approach to Gaussian process inference requires matrix algebra to manipulate the multivariate Gaussian distribution in Eq. (4), requiring $\mathcal{O}(n^3)$ time and $\mathcal{O}(n^2)$ storage. In Flaxman [2014], n was the number of space-time locations, that is, 77 neighborhoods times 156 weeks (3 years) for a total of $n = 12,012$. This is at the limit of what is possible without more sophisticated methods, e.g. storing a $12,012 \times 12,012$ covariance matrix requires about 1 gigabyte of ram but Flaxman et al. [2015] consider a dataset for which $n > 1e6$, meaning it would require at least 8 terabytes to store the covariance matrix in memory, which is clearly infeasible. Much work in spatial statistics and machine learning has focused on alleviating this computational burden, with the most popular methods including various types of inducing points [Snelson and Ghahramani, 2006, Titsias, 2009], low-rank approximations to the kernel matrix [Williams and Seeger, 2001], and finite-dimensional approximations to the kernel itself [Quiñonero Candela et al., 2010, Rahimi and Recht, 2007]. In the case of spatiotemporal point pattern data in which inference proceeds assuming that the data has been discretized to a computational grid [Diggle et al., 2013], a very effective approach is to use Kronecker algebra, which exploits the Cartesian product nature of the grid (space \times time) and the separable structure of the kernel [Saatçi, 2011, Gilboa et al., 2013, Wilson et al., 2014, Flaxman et al., 2015].

As mentioned above, Flaxman et al. [2015] aim to learn, rather than specify, an interpretable kernel that is able to represent patterns in the data. For this purpose, they use the recently proposed Spectral Mixture (SM) kernel [Wilson and Adams, 2013], and show that they are able to uncover interpretable temporal periods in the data, and also spatially varying temporal trends. In terms of accuracy, this means that the proposed model is able to obtain accurate long range forecasting, but at a finer-grained spatial scale, and without feature engineering.

Flaxman [2014] and Flaxman et al. [2015] both demonstrate that it is possible to forecast aggregate small area crime rates far into the future under the following conditions: the crime type is relatively abundant, forecasts are made weekly, and the main trend explaining the crime rate can be decomposed into (spatially varying) secular and a periodic time trends. We note that the forecasting challenge we describe here is not necessarily characterized by these features: the task is not weekly long range forecasting (i.e. what will happen in 12 weeks in this neighborhood?) but cumulative long range forecasting (starting tomorrow and aggregating over the course of the next two months, what will be the crime rate?), so learning periodic / seasonal trends is not important. Further, as discussed below, the evaluation metric focuses on hotspot forecasting, whereas the previous papers were focused on learning an accurate intensity surface across the entire city, in both high- and low-crime areas. Nevertheless, the flexibility of this kernel-based approach, suggests that this approach could also be well-suited to these additional forecasting situations.

2.3 Scalable kernel methods

As mentioned above, the matrix algebra operations required for calculations involving multivariate Gaussians are not scalable to large datasets. Practitioners face the same issue when applying nonlinear kernel methods [Schölkopf and Smola, 2002], as they rely on the calculation and manipulation of an $n \times n$ Gram matrix, which

corresponds exactly to the covariance matrix parameterized by the covariance kernel in Gaussian processes. While a variety of approaches have been proposed to alleviate this computational difficulty, including low-rank approximations [Williams and Seeger, 2001], we consider random Fourier features [Rahimi and Recht, 2007, 2008] due to the simplicity with which it can be embedded within a larger supervised learning framework.

Random Fourier Features are a randomized approximation yielding a finite-dimensional feature mapping (and corresponding finite-dimensional Reproducing Kernel Hilbert Space) which approximates the original kernel. Proposed in 2007 [Rahimi and Recht, 2007] and marketed as only requiring 3 lines of MATLAB code to apply, the authors won a “Test of Time Award” at NIPS in 2017 for their widespread applicability and elegance.

Recall Bochner’s theorem (for a precise statement in multiple dimensions see [Stein, 1999, p. 24]), which establishes a one-to-one correspondence between a stationary kernel $k(x_i, x_j) = \kappa(x_i - x_j)$ and a positive finite measure μ . In particular, κ is the Fourier transform of μ :

$$\kappa(x - y) = \int_{\mathcal{R}} e^{i\omega^\top(x-y)} d\mu(\omega) \tag{7}$$

Recognizing that this infinite dimensional integral is an expectation over the measure μ suggests that it can be approximated using Monte Carlo sampling. Consider iid samples:

$$\omega_1, \dots, \omega_d \sim \mu(\omega) \tag{8}$$

Then we have the following approximation, where we ignore the imaginary component since we only care about real-valued kernels:

$$\kappa(x - y) \approx \frac{1}{d} \sum_{j=1}^d e^{i\omega_j^\top(x-y)} \tag{9}$$

$$= \frac{1}{d} \sum_{j=1}^d \cos(\omega_j^\top(x - y)) + i \sin(\omega_j^\top(x - y)) \tag{10}$$

$$= \frac{1}{d} \sum_{j=1}^d \cos(\omega_j^\top x) \cos(\omega_j^\top y) + \sin(\omega_j^\top x) \sin(\omega_j^\top y) \tag{11}$$

$$= \langle \Phi(x), \Phi(y) \rangle \tag{12}$$

where we can define an explicit feature mapping $\Phi : \mathcal{X} \rightarrow \mathcal{R}^{2d}$ consisting of the following pairs of elements concatenated together:

$$\Phi_j(x) = \frac{1}{\sqrt{d}} \begin{pmatrix} \cos(\omega_j^\top x) \\ \sin(\omega_j^\top x) \end{pmatrix}$$

The elegance of random Fourier features is that in a supervised learning setting with n observations and p covariates with design matrix $X \in \mathcal{R}^{n \times p}$, we can immediately consider introducing kernel-based nonlinearities, without changing our learning approach, simply by transforming our design matrix into $[\cos(X\Omega^\top) \quad \sin(X\Omega^\top)]$ for a set of random frequencies $\Omega \in \mathcal{R}^{d \times p}$ (here, $\cos(A)$ is not the matrix Taylor expansion of the matrix A ,

but the element-wise computation of cosine on A). In homage to the three lines of MATLAB code, three lines of R code are shown below to transform a design matrix X into a new design matrix Φ assuming a squared exponential kernel with lengthscale 1, $k(x, y) = \exp(-.5\|x - y\|^2)$:

```
Omega = matrix(rnorm(d*ncol(X)), d)
Proj = x %*% t(Omega)
Phi = cbind(cos(Proj), sin(Proj)) / sqrt(d)
```

Changing the covariance kernel to, for example, the Matérn kernel requires simply sampling from a Student-t distribution instead of a normal distribution. At this point, any (suitably regularized) linear learning method can be applied to Φ : ridge regression with Φ is an approximation to kernel ridge regression with X ; Bayesian linear regression with Φ is an approximation to Gaussian process regression with X .

3 Previous work on spatiotemporal forecasting

Both time series and spatial statistics separately have very long and very well-developed literatures with a variety of well-known and popular methods, with too many to summarize here. See [Box et al., 2015, Brockwell and Davis, 2013] for its comprehensive coverage of time series and [Cressie, 1993, Cressie and Wikle, 2011, Ripley, 1981, Diggle, 2013] for spatial statistics. Despite these impressive bodies of work, the field of spatiotemporal statistics, which unites the two, remains nascent, with the state-of-the-art summarized in [Cressie and Wikle, 2011]. Strikingly, the specific problem of generic spatiotemporal forecasting is one that has received some attention within various application areas, but for which few generic methods have been proposed. The most well-developed methods have been proposed for environmental forecasting, see, for example, [Hering and Genton, 2010, Sahu and Bakar, 2012, Xie et al., 2011].

Methods which could enable spatiotemporal forecasting (even if this feature is not often explicitly addressed) can be broadly categorized as stemming either from time series methods or from spatial methods. On the time series side, autoregressive / state-space models have been used where a vector of spatial observations evolves over time with an autoregressive structure. See [Martin and Oeppen, 1975] for an early example in the literature which describes the Space-Time Autoregressive model, the Space-Time Moving Average model, and more, and see [Stroud et al., 2001, Tonellato, 2003] for more recent examples. A related example is the location-mixture autoregressive process (LMAR) [Cervone et al., 2014].

On the spatial side, forecasting is again not usually discussed. Huang and Cressie [1996] combine kriging with the Kalman filter for spatiotemporal interpolation, while [Wikle et al., 1998] and [Cressie and Wikle, 2011] promote the use of hierarchical Bayesian models for spatiotemporal data, combining Gaussian process-type models for spatiotemporal variation with location specific time series models. Foreman et al. [2017] explicitly focuses on forecasting: the authors combine a hierarchical Bayesian modeling approach with the Conditional Autoregressive model (CAR) for small area mortality forecasting.

In addition to methods rooted in the spatial or time series literature, the statistical machine learning

literature contains several interesting approaches, for example [Goerg and Shalizi, 2012, Montañez and Shalizi, 2017, Bahadori et al., 2014]. Also of note are a Bayesian nonparametric approach [Aldor-Noiman et al., 2013] and deep neural network approach [Kang and Kang, 2017] to crime forecasting specifically. We discuss spatiotemporal crime forecasting in more detail below.

3.1 Spatiotemporal crime forecasting

For at least the last 70 years, pin-maps formed the basis of spatial crime forecasting [Schutt, 1922, Bratton, 1998]. Prior week’s crimes were mapped and qualitative assessments of density, location, stability and significance were made. These maps were complemented by simple time-series charts aggregating reported crime counts by somewhat arbitrarily selected jurisdictional boundaries such as census tracts or patrol boundaries. This approach began to change with the introduction of geographic information systems in the 1990s, enabling the routine application of the basic tools of spatial statistics to the problem of predicting crime patterns. Early crime forecasting approaches tested a range of different methodologies [Gorr et al., 2003], often finding that the small areas being forecasted were characterized by high degrees of random noise. While a variety of approaches were proposed for resolving this signal-to-noise problem, the most consistently productive approach became kernel density estimation [Gorr and Lee, 2015, Porter and Reich, 2012, Boni and Gerber, 2016].

In recent years, due in part to criminological theories and empirical evidence of elevated levels of near-repeat victimization [Pease et al., 1998], particularly for burglary, several authors have also proposed and implemented self-exciting point process models [Levine, 2004, Liu and Brown, 2003, Taddy, 2010, Mohler et al., 2011, Rosser and Cheng, 2016]. These models have been shown to often but not always outperform KDE methods [Mohler et al., 2011, Rosser and Cheng, 2016]. While only a handful of studies have compared the most common type of point process model to KDE, it appears that the accuracy gains from point process models are generally larger than reported accuracy gains for KDE-only models that supplement historical crime data with additional sources of both static and dynamic information [Wang et al., 2012, Gerber, 2014, Al Boni and Gerber, 2016].⁴ Like the larger spatiotemporal forecasting literature, the models most commonly used (e.g., KDE surfaces) are often implemented outside of a supervised learning framework. This has meant that for any given model, features, weighting, bandwidths, and virtually every other model parameter has been set based on trial-and-error or theory rather than through a systematic search of optimal parameters for forecasting accuracy. For high volume events, this optimization may not be particularly necessary, but this is less likely to be the case for low volume events or high volume events over very short time periods.

⁴Criminologists have also reported using census, administrative, and other records to create a risk surface that outperforms predictions from naive retrospective KDE surfaces [Caplan et al., 2011, Kennedy et al., 2011]. This accuracy improvement given the use of mostly static factors merits further exploration. One possible explanation may be the exclusion of always zero locations from consideration by the risk enhanced models conditioned on covariates.

4 Our model

We first present the hypothetical model we would use if computational constraints were not a concern, then we present our actual model, which is an approximation to this model. Our hypothetical model is a log-Gaussian Cox Process, meaning that it is a doubly stochastic model which we parameterize hierarchically as follows:

$$f \sim \mathcal{GP}(\mu, k_\theta(\cdot, \cdot)) \quad (13)$$

$$N(S)|f \sim \text{Poisson}\left(\int_S \exp(f(\mathbf{s}))d\mathbf{s}\right) \quad (14)$$

$N(S)$ is a counting measure—a discrete random variable—giving the number of points in space-time volume S . $f(\mathbf{s})$ is real-valued, so to use it as the rate parameter in a Poisson distribution, we need to transform it to be non-negative. The choice of an exponential link function means that we are placing a Gaussian process prior on the log-intensity, thus the name log-Gaussian Cox Process. To complete the specification, we would need to parameterize μ and k_θ . Inference with this model is difficult because it is doubly intractable and existing approaches

[Møller et al., 1998, Brix and Diggle, 2001, Cunningham et al., 2008, Adams et al., 2009, Teh and Rao, 2011, Diggle et al., 2013] are often limited to one dimension and small datasets. [Lloyd et al., 2015] is a possible exception in that it points the way to a scalable stochastic variational inference approach.

Now we turn to our model, an approximation to the model above. Our first approximation requires the specification of a space-time grid covering S . We assume that the grid has N cells, each indexed by its centroid given as a latitude/longitude/timestamp triple $\mathbf{s}_i = (x_i, y_i, t_i)$. Now instead of a point pattern we consider our dataset as aggregate counts o_i of the number of crimes per grid cell. Given a grid, we can now approximate the integral in Eq. (14) with a sum:

$$\int_S \exp(f(\mathbf{s}))d\mathbf{s} \approx \frac{1}{N} \sum_{i=1}^N \exp(f(\mathbf{s}_i)) \quad (15)$$

In a Poisson process, conditional on the intensity, the random variables $N(S_1)$ and $N(S_2)$ are independent for $S_1 \cap S_2 = \emptyset$. Thus we can consider each grid cell S_i , so Eq. (14) becomes:

$$o_i|f \sim \text{Poisson}(\exp(f(\mathbf{s}_i))) \quad (16)$$

We can treat this as an iid likelihood (observation model) over all cells i , and we arrive at the so-called computational grid approximation to the log-Gaussian Cox Process [Diggle et al., 2013, Flaxman et al., 2015].

However, our approximation is not complete. To further enable a highly scalable model, we use an approximation to f which will allow us to avoid multivariate Gaussian algebra altogether and easily enable stochastic gradient descent for inference. As introduced in the Section 2.3, we consider the random Fourier feature expansion of a reproducing kernel Hilbert space \mathcal{H}_k . For any stationary kernel k , there is a corresponding spectral density Λ , and we draw a set of frequencies $\omega_1, \dots, \omega_m$ from this density where we choose a

larger m to improve the approximation. The lengthscale parameter θ of the kernel corresponds to the variance of Λ , and we will choose it by crossvalidation. With an explicit feature expansion, we no longer have to worry about the algebra involved in working with realizations f from a multivariate Gaussian prior; instead, we can use the machinery of generalized linear modeling (GLM) as we are now dealing with a regression problem where we want to learn coefficients β for covariates given by a particular design matrix Φ containing the random Fourier features (cos and sin terms from Eq. (11)). Thus we have the following GLM with Poisson likelihood and exponential link function:

$$o_i | \beta, \mu, \Phi \sim \text{Poisson}(\exp(\mu + \Phi\beta)) \quad (17)$$

It remains to specify the function μ . One choice would be to simply use $\mu = 0$, but we know from previous work that using historical rates can be very effective in crime forecasting. Another simple approach would be to follow the use of e_s in Eq. (6) and fix μ as piecewise constant, estimated from historical data and not time-varying. We use a more flexible parametric model, in line with our overall supervised machine learning approach and with previous work on crime forecasting using heatmaps.

$$\mu(x, y, t) = \sum_{i=1}^p \gamma_i \text{KDE}_{\lambda, i}(x, y) \quad (18)$$

where we have p lagged terms, each representing a spatial heatmap for a given time period in the past and we wish to learn regression coefficients γ_i . $\text{KDE}_{\lambda, i}(x, y, t)$ is the kernel density estimator at location (x, y, t) using a Gaussian kernel κ_λ which ignores time with spatial lengthscale λ :

$$\text{KDE}_{\lambda, i}(x, y, t) = \sum_{\{t_j \mid t-i \cdot d < t_j \leq t-(i-1) \cdot d\}} \kappa_\lambda((x, y), (x_j, y_j)) \quad (19)$$

where d is the size of the temporal window in days.

Combined with a Poisson likelihood and with observations o_1, \dots, o_n , we have specified a problem which is amenable to solving by maximum likelihood. Since we have the potential for a very large number of parameters (the more random frequencies m we choose for the random Fourier feature expansion, the better our approximation) we consider the use of ℓ_1 and ℓ_2 regularization, as in the popular elastic net [Zou and Hastie, 2005]. The parameters of the model are β and γ , and we learn these by maximizing the likelihood of our model using gradient descent, as implemented in the large-scale machine learning package Vowpal Wabbit⁵. In particular, we fit the training dataset described in Table 1 using the Poisson likelihood as loss function, default settings for the learning algorithm (a variant of online gradient descent) and default settings for the learning rates, with at most 200 training passes (epochs) through the dataset. After fitting the model, we make predictions in the form of counts for the test data from Table 1, and then calculate PEI for each year of data.

To learn the hyperparameters we maximize average PEI. The hyperparameters related to our model are as follows: the number of random frequencies d , the number of lags p , the size of the temporal window d , the spatial lengthscale for KDE λ , the covariance kernel lengthscale θ , and the amount of ℓ_1 and ℓ_2

⁵<http://hunch.net/~vw/>

regularization. In addition, there are hyperparameters related to the data and forecasts: cell size, shape, grid rotation, and forecast area, which we also learn by crossvalidation. We considered a very large grid search over hyperparameters, supplemented with Bayesian Optimization [O’Hagan, 1992, Snoek et al., 2012, Hennig et al., 2015]. The details of the hyperparameters we selected are given in the Appendix in Section A.1.

All of our computation was carried out on in a parallel cluster computing environment, with 8 Dell PowerEdge R630 nodes consisting of $2 \times$ Intel Xeon E5-2690 v4 2.6 GHz, 14 Core CPUs, and 256 GB memory.

4.1 Relationship with other work

The intuition behind our approach is that we combine state-of-the-art nonparametric spatiotemporal methods (Gaussian process regression) with the most long-standing and widely used crime forecasting method (heatmaps) by defining sets of features for each. We then place these two sets of features into a supervised learning framework for forecasting the intensity, and consider a large set of hyperparameters and training data, with the hope that we will be able to obtain good predictive performance on unseen data. In this section, we detail the connections between our kernel density estimation (KDE) features and the Hawkes process [Ogata, 1988, Møller and Rasmussen, 2005, Mohler et al., 2011, Mohler, 2014, Rosser and Cheng, 2016, Loeffler and Flaxman, 2017]. The conditional intensity function used in a spatiotemporal Hawkes process takes the following form:

$$\lambda(x, y, t) = \lambda_0(x, y, t) + \sum_{\{j|t_j < t\}} k_t(t_j, t) \cdot k_s((x_j, y_j), (x, y)) \quad (20)$$

where the first term is an underlying (endogeneous) intensity and the second term is the self-excitatory component and we assume that we have the same dataset as in the previous section. An illustration is shown in Figure 3 in black for a temporal process with exponential kernel k_t : whenever an event occurs, the intensity increases, followed by exponential decay. This is in contrast to the kernel-smoothed intensity shown in blue for a temporal process with the intensity fit with KDE (actually, as we are estimating an intensity, not a density, this is technically known as kernel intensity estimation.) KDE is a nonparametric smoothing method which does not take the directionality of time into account, so the intensity rises before and after an event occurs. This seems like a critical difference, and the shape of the intensities in Figure 3 are clearly different. But as we see below, our use of KDE features in a forecasting framework corresponds exactly to what we could obtain using an analogous set of “Hawkes features” (the terminology comes from another team’s submissions to the competition [Mohler and Porter, 2017]).

$$\text{KDE}_{\lambda,i}(x, y, t) = \sum_{\{t_j \mid t-i \cdot d < t_j \leq t-(i-1) \cdot d\}} \kappa_{\lambda}((x, y), (x_j, y_j)) \quad (21)$$

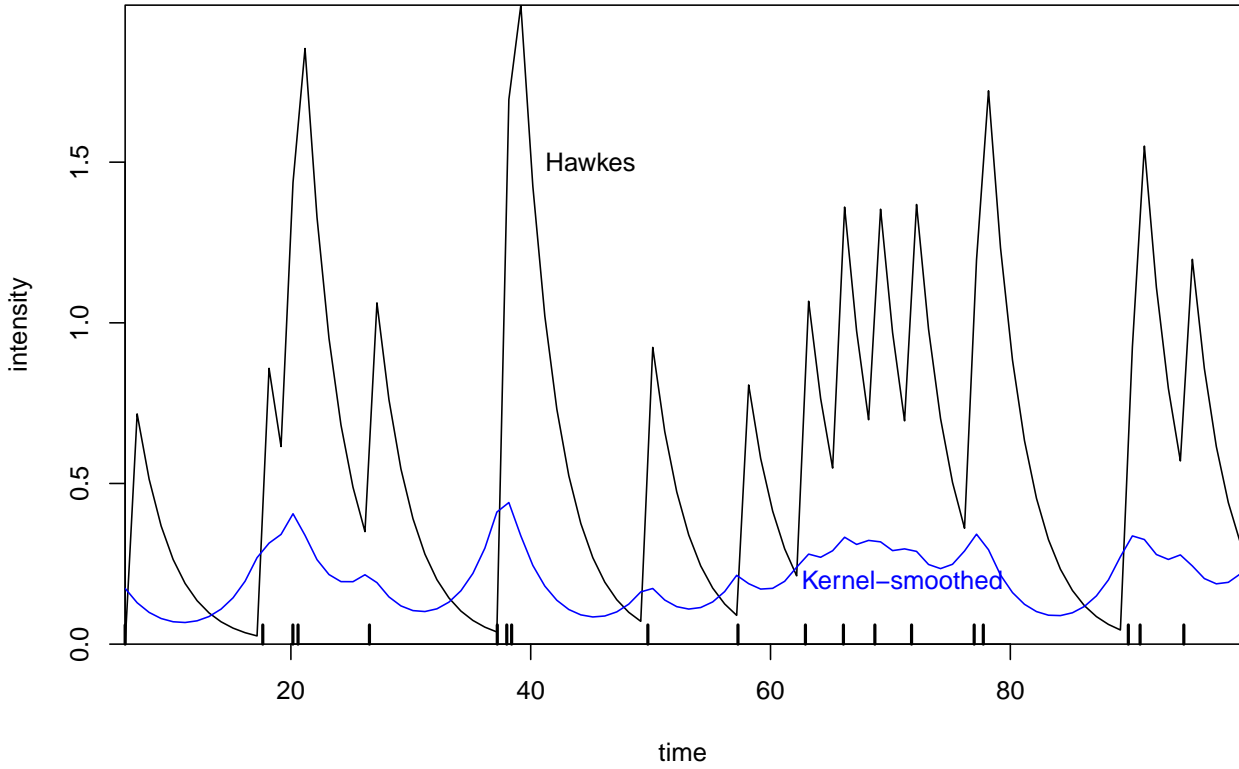


Figure 3: Hawkes intensity vs kernel-smoothed intensity on a synthetic dataset. The Hawkes intensity is explicitly self-exciting while kernel smoothing does not take the directionality of time into account.

As defined in Eq. 21, $\text{KDE}_{\lambda,1}(x, y, t)$ is the lag-1 spatial kernel density estimator at location (x, y) using data with time labels $\in [t - d, t]$, i.e.:

$$\text{KDE}_{\lambda,1}(x, y, t) = \sum_{\{j|t_j \in [t-d, t]\}} k_s((x_j, y_j), (x, y)) \quad (22)$$

If we consider Eq. (20) and the special case in which

$$k_t(t_j, t) = \begin{cases} 1 & \text{if } t_j \in [t - d, t] \\ 0 & \text{otherwise} \end{cases} \quad (23)$$

we see that the KDE feature is equivalent to the self-excitatory term in the Hawkes process conditional likelihood. How do we thus understand this equivalence in light of Figure 3? Within our forecasting framework, the past intensity is a feature that is used to forecast the future number of crimes. Since our KDE estimate of the intensity cannot take future data into account (since from the point of view of the features, the future

has not occurred yet), we recover the directionality of time which was explicit in the Hawkes approach.

The kernel in Eq. (23) is rather simplistic, suggesting an obvious extension to our method of including a more interesting temporal kernel in the KDE features of Eq. (22) and possibly also for other lags as in Eq. (21).

5 The competition

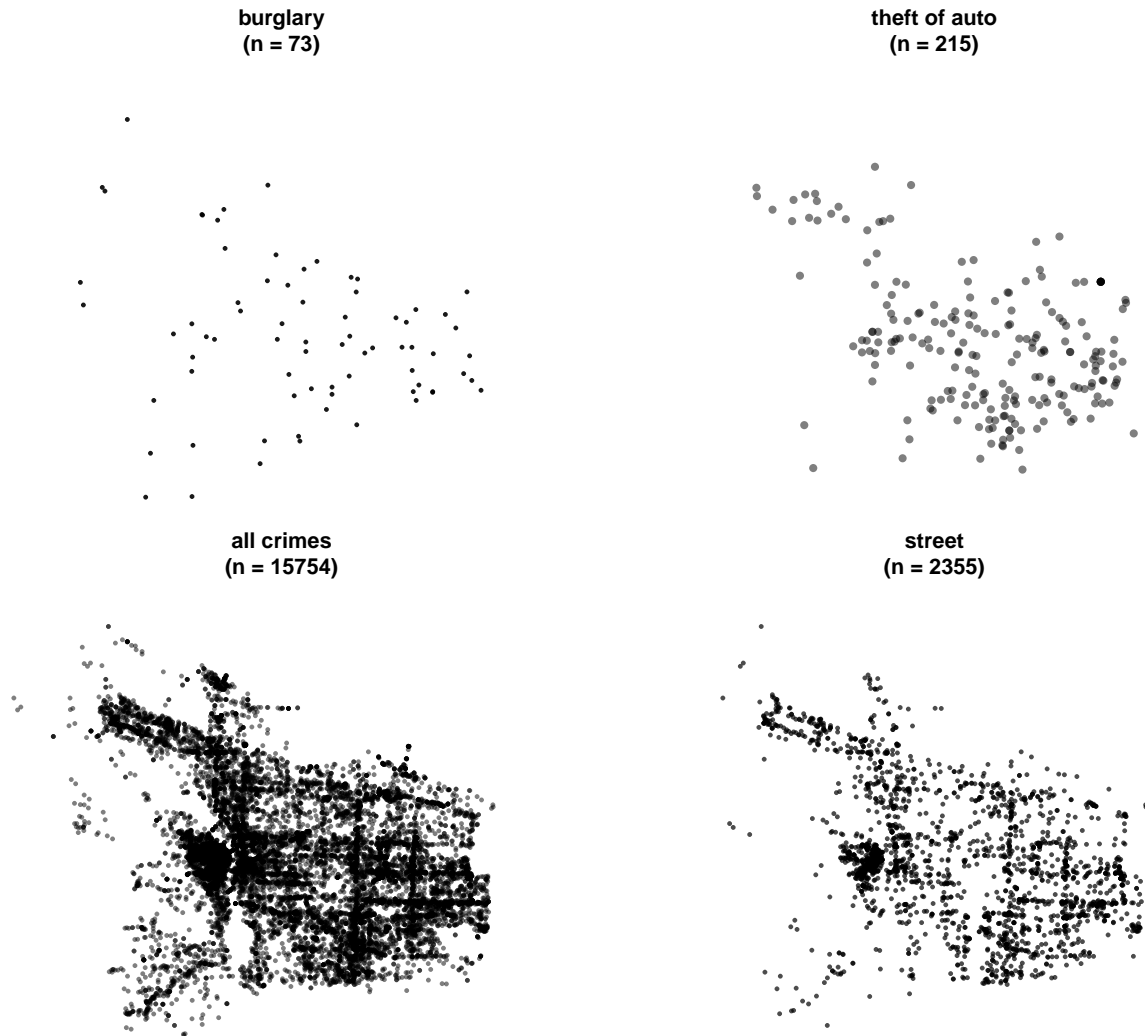


Figure 4: The competition focused on four categories of crimes, ranging from the very abundant (all crimes) to the very sparse (burglaries). Shown here are the locations of reported crimes in February 2016.

5.1 Data and Setting

The NIJ Real-Time Crime Forecasting dataset consists of 958,499 calls-for-service records from the Portland Police Bureau (PPB). These spatiotemporal records represent calls to Portland’s 911 system requesting police assistance from March 1st 2012 through February 28th, 2017.⁶ On average, there were 2.6 burglary calls per day, 6.8 motor vehicle theft calls per day, 93 street crime calls per day, and 470 other calls per day for a total of 572 calls for service per day. As shown in Fig. 4, the four categories of crime, which themselves varied in the degree of internal heterogeneity, included Burglary (Burglary and Prowling), Street Crime (ranging from Disturbance and Threats up to Armed Robbery and Assault with a Firearm), theft of Auto, and all calls for service. With a handful of exceptions⁷, this covered all calls for service routed to the Police Bureau during this period.

5.2 Metrics

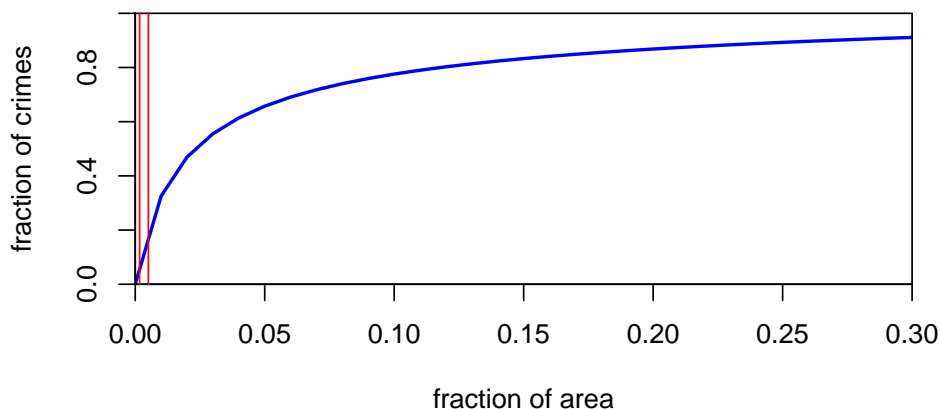


Figure 5: A standard approach to crime forecasting is to analyze a Receiver Operating Characteristic (ROC) curve as illustrated here using synthetic data with the fraction of total area of the city covered on the x axis and the hit rate or fraction of crimes predicted on the y axis. The NIJ crime forecasting challenge focused on a very narrow range of this curve, covering between 0.2% and 0.5% of the total area of the city.

For a particular forecasting period, say one week into the future, the simplest metric that has been

⁶In practice, the final day of pre-competition data was not posted via NIJ’s website until after the submission deadline. Via web-scraping of twitter posts of PPB calls for service, a portion of this final day’s calls were incorporated into forecasts.

⁷The following calls-for-service were excluded (primarily violent crimes): administrative, arson, crisis, death, domestic disturbance/violence, juvenile offenses, kidnapping, K9 explosive sweep, missing person, rape, restraining order, sex offense, stalking, and suicide. In addition, a handful of locations were also excluded (all hospitals and police precincts): 737 SE 106th Ave (East Precinct), 449 NE Emerson St (North Precinct), 2801 N Gantenbein Ave (Legacy Emanuel Hospital), 4804 NE Glisan St (Providence Hospital), 1111 SW 2nd Ave (Central Precinct), 10300 SE Main St (Adventist Medical Center), 1014 NW 22nd Ave (Legacy Good Samaritan Medical Center), 41 NE Grand Ave (Detox Center), 3181 SW Sam Jackson Park Rd (OHSU Hospital), 10123 SE Market St (Adventist Medical Center), 12240 NE Glisan (Multnomah County Sheriffs Office), and 3303 SW Bond Ave (OHSU Hospital)

proposed in the criminological literature is the “hit rate” [Chainey et al., 2008b]⁸:

$$\text{Hit rate} = \frac{n}{N}$$

where n is the number of crimes predicted and N is the total number of crimes in that period. The hit rate is simply the fraction of crimes predicted. A more standard statistical term would be sensitivity. As shown in Fig. 5 this will depend critically on the size of the forecasted area. Thus, crime forecasting models are often evaluated based on ROC performance assessed over the entire region of interest, so hit rate can be compared to fraction of area as in the figure. For more on ROC, see [Gorr, 2009].

However, ROC/AUC metrics are not well-suited for assessing the accuracy of forecasting models for crime hotspots that often cover only a very small fraction of a particular jurisdiction. In the case of the NIJ competition, this coverage area was between 0.2% and 0.5% of the City of Portland, which means that if we did consider an ROC curve we would be restricting ourselves to a very small portion of it, namely the region between the red vertical lines in Fig. 5.

The NIJ competition focused on two recently proposed alternatives to AUC [Chainey et al., 2008b, Hunt, 2016], with a goal similar to ROC/AUC analysis insofar as they purportedly allowed for the comparison of hit rates across different coverage areas. But unlike a standard use of ROC or AUC, where the coverage area would be prescribed as a fixed set or range, the NIJ competition required teams to choose a coverage area so as to maximize performance on the PEI and PAI metrics. Thus teams were allowed to decide how much of the allowable forecasted area (.25-.75 sq miles) to cover with their predictions—a decision affected both by coverage area, underlying crime densities, and forecasting quality. The prediction accuracy index (PAI) [Chainey et al., 2008b] is defined as the ratio of the hit rate to the fraction of area covered:

$$\text{PAI} = \frac{\frac{n}{N}}{\frac{a}{A}}$$

The idea is that this objective trades off hit rate and coverage.⁹

The prediction efficiency index (PEI) is defined as the ratio of PAI to the hypothetically maximum PAI that could have been obtained using the submitted grid and forecasting area. Since the forecasting area is the same in both cases, this reduces to:

$$\text{PEI} = \frac{n}{n^*}$$

Where n is the number of crimes occurring in predicted hotspots, and n^* is the maximum number of crimes that could have been captured for the forecasted area.

For sparse crimes at some horizons, $n^* = N$, the totality of crimes in that category. For example, in all of the training periods’ one-week horizons (March 2016, March 2015, etc.), there were only a small number

⁸See Adepeju et al. [2016] for a recent discussion of alternative evaluation metrics for crime forecasting.

⁹Note, however that the weighting of this tradeoff implicitly weights as equal the following: a multiplicative increase in the sensitivity and a multiplicative decrease in the forecasted area. This can be seen with a simple example: consider a sensitivity (hit rate) of 10% for a forecasted area covering 0.4% of the city. The PAI is 25. If we doubled the sensitivity to 20% or halved the forecasted area to 0.2% of the city PAI would equal 50.

of burglaries or motor vehicle thefts (15 and 43 respectively each week). This is because, for such a small number of crimes, even a tiny forecasted area (e.g., the minimum of 62,500 sq. ft), ideally, would be able to cover every single incident. By contrast, for crimes which see 100s or 1000s of occurrences in a given horizon (street crimes in Portland typically measure 650 all calls-for-service measure 3690), no matter how the hotspots are arranged, there will be missed crimes since there is a maximum forecasted area ($\bar{A} = 360,000$ sq. ft). That means that the way to maximize *PEI* is to try and cover every crime that will occur in the designated hotspots.

Therefore, for relevant crime and horizons, we eliminated the forecasted area as a hyperparameter, since (in expectation) any forecast for an area less than \bar{A} could be improved by simply forecasting more hotspots¹⁰. This optimization, however, comes with a trade-off. Optimizing for *PEI* in this manner incurs a *PAI* penalty proportional to the marginal change in forecasted area divided by the marginal change in correctly forecasted crimes. As the expectation of correctly predicting crime(s) in the marginal cell shrinks geometrically, the denominator continues to grow linearly. Therefore, the optimal cell selection for maximizing *PEI* will often fail to maximize *PAI* and visa-versa. We therefore somewhat arbitrarily decided to maximize *PEI* rather than *PAI*. [Note: For a result making the opposite choice, see [Mohler and Porter \[2017\]](#).]

5.3 Data for training and hyperparameter selection

There are various ways in which the raw data can be transformed to create a supervised learning problem. For a given time horizon and crime type, we are required to submit a map of hotspots, which is then scored on both the *PEI* and *PAI* metrics. We consider a range of spatial grid sizes, but restrict our temporal grids to match the forecasting window, so our data is aggregated to the weekly level for one week forecasts, the monthly level for the monthly forecasts, and so on. Ideally, we want to consider training datasets which are each as close to the real task as possible. We adopted the following approach, which we show for the 1 week horizon forecasts for simplicity in Table 1. We create a single dataset using data from the union of all of the

Training period	Test period
28 September 2012 - 28 February 2013	1-8 March 2013
28 September 2013 - 28 February 2014	1-8 March 2014
28 September 2014 - 28 February 2015	1-8 March 2015
28 September 2015 - 28 February 2016	1-8 March 2016

Table 1: Train/test split for the 1 week time horizon

training periods in Table 1.¹¹ We train the parameters of our model, as detailed in the next section, using this dataset. Then we produce forecasted hotspot maps for the five different test periods in Table 1 and calculate *PEI* and *PAI* for each. We then report average heldout *PEI* and *PAI*, and it is these metrics that we maximize (in particular *PEI*) to select the hyperparameters of the model.

¹⁰We ignore the possibility that the optimal cell area is a such that $ka < \bar{A} < (k+1)a$

¹¹In the competition, to produce a more robust model, all years of data were weighted equally. However, inverse weighting by temporal distance could produce additional benefits, especially for less stochastic event patterns. Similarly, in competition, the most recent and incomplete dataset for late 2016 and early 2017 was excluded from training the hyperparameters.

Portland, like many cities, has a mix of north/south and east/west aligned streets. However, it also has a non-trivial number of obliquely-oriented streets and parcels. This is especially the case in downtown Portland, east of the Willamette River and south of West Burnside Street. Given the concentration of calls-for-service in this area, it seemed likely that a non-standard alignment could be beneficial, especially for all calls-for-service. For this reason, grid angle of rotation was included as another parameter to be learned by the model, an idea first proposed by [Johnson et al., 2009]. Non-uniform land use coupled in Portland with the common

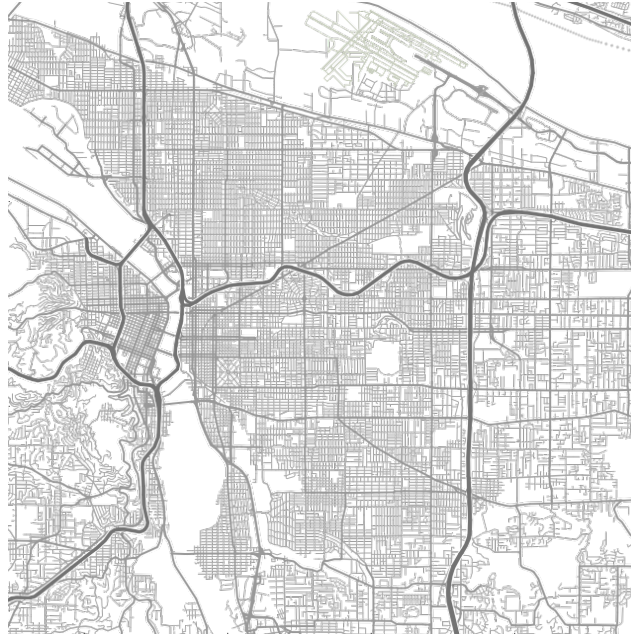


Figure 6: Central Portland

practice of geocoding crime data to the street grid suggested that a fixed N/S oriented square tessellation could be sub-optimal [Rosser et al., 2016].¹² However, contest rules required that shapes be polygons that could be tessellated without rotation. While squares were the simplest choice, the nature of the calls-for-service data geocoded to the street grid suggested that rectangles could be preferable¹³. For this reason, we chose to leave the cell shape as a parameter to be optimized with each crime type and forecasting period potentially receiving its own optimized solution. Similarly, contest rules permitted a variety of different cell sizes and consistent with recent working demonstrating the sensitivity of forecast accuracy to cell size [Hart and Zandbergen, 2014], we left this as a parameter to be optimized.

¹²Data provided by NIJ included calls geocoded to the building footprints and then offset several feet onto the street grid directly in front of the relevant address.

¹³We also considered the other regular tessellations of the plane – namely, equilateral triangles and regular hexagons. Both suffered from computational problems, as no extant open libraries offer scalably-fast kernel density estimation over non-rectangular polygons. Nevertheless, some firms (notably Uber) use hexagons at scale for spatiotemporal forecasting.

6 Results

In this section we describe the performance of our method according to the particularities of the NIJ challenge, assess its robustness on a larger class of similar tasks, and investigate what features of the model contributed to its performance.

6.1 NIJ Challenge Results

There were a total of 20 categories (4 crime types and 5 forecasting windows) but 40 winners were selected, one for PEI and one for PAI in each category. We won a total of 9 categories in the “Large Business” competition. As we focused on maximizing average forecasted PEI, most of our winning entries were in this category: all crimes (1 week, 1 month, 3 months), burglary (1 week, 2 weeks), street (2 weeks), and vehicle (1 week). We also had winning PAI entries for burglary (1 week and 2 weeks).

Based on these overall results we first investigate the two metrics, PEI and PAI. PEI and PAI clearly measure different things, because maximizing PEI did not usually lead to maximizing PAI or visa-versa. But of course they are related: the Pearson’s correlation between the two metrics by crime type and period ranged from 0.85 to 0.99 with particularly high correlations for all crimes and street crimes, the higher frequency crime types. Indeed, as the forecasting period lengthened the correlation increased as well, from 0.55 for all 1 week forecasts to 0.95 for all 3 month forecasts. Note that this does not explain our simultaneous winning entries for burglary in the PAI and PEI categories at 1 week and 2 weeks, an issue we consider more detail below.

Next we investigate the hyperparameters that were selected by our hyperparameter search strategy (grid search and Bayesian Optimization side-by-side). As shown in the Appendix in Table A.1, there were no consistently chosen hyperparameter values: the grid cells were sometimes small squares 250ft \times 250ft (the minimum area) or large squares 600ft \times 600ft (the maximum area) or large rectangles 800ft \times 450ft (also the maximum area). The coverage fraction ranged from the minimum (0.25 sq miles) to the maximum (0.75 sq miles). The lengthscales for space and time were all over the place, as were the number of KDE lags and the KDE bandwidth. Interestingly, the number of random Fourier features went as low as 5, which means that the surface was a very crude approximation to a Gaussian process consisting of the sum of 10 random sine and cosine functions to as high as 362, a much better approximation. In many cases, no ℓ_1 or ℓ_2 regularization was needed. In a minority of cases (4 out of 20) the hyperparameters were chosen by Bayesian Optimization, while the rest were the result of the grid search. Note that the grid search considered many many more combinations of hyperparameters, as the vanilla Bayesian Optimization approach did not make use of parallel computing. While it is clear from Table A.1 that the performance depended on optimizing the hyperparameters, the question remains how strong was this dependence, i.e. were there many reasonable choices for the hyperparameters. As one means of assessing this question, we considered the distribution of PEI values for each crime category and forecasting window and used this distribution to calculate the z-score of each maximum. In all crimes, the z-scores ranged from 2.5 to 4.0. In street the z-scores ranged from 2.8 to 5.6. In vehicle the z-scores ranged from 7.5 to 21. In burglary the z-scores ranged from 6.2 to 12.4. In many

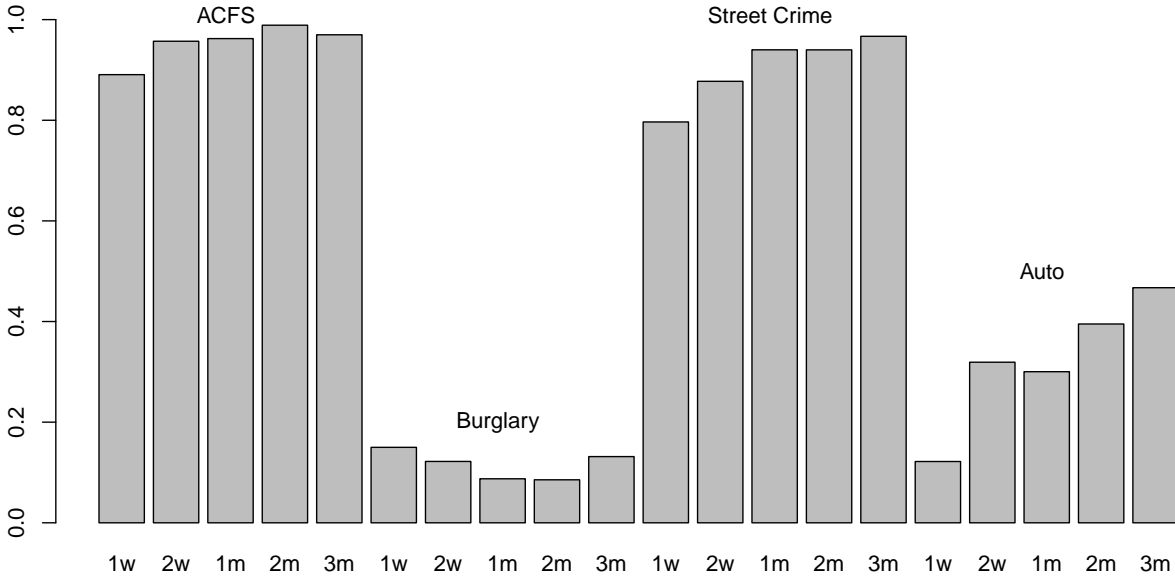


Figure 7: Competition Max. PEI Performance (All Competitors)

cases, the particularly high z-scores corresponded to winning entries, e.g. our winning vehicle 1 week entry had a PEI z-score of 21, and our winning burglary entries had z-scores of 12.4 (1 week) and 11 (2 weeks). This supports the idea that there was a particularly good set of hyperparameters found by our grid search. Such high z-scores might lead to a worry about overfitting, but the fact that these entries were often winning entries is reassuring. Note also that these high z-scores are explained in part by the relative frequency of hyperparameters which led to PEI scores of 0: for the 1 week vehicle and burglary categories, 41% and 44% (respectively) of the possible hyperparameter combinations gave PEI scores of 0.

As shown in Figure 7, which depicts the competition PEI maximums, for high volume crimes, such as all calls for service, even a week’s worth of data is sufficient to achieve very high PEI scores (nearly 0.9) of the theoretical limit (1) for a one week prediction. Extending the forecast period leads to further improvements in forecasting accuracy, plateauing at 97%. Sizable sub-categories, such as street crimes, share this basic trajectory as well. For some sparse crimes, such as motor vehicle theft, despite lower starting values, similar improvements in predictive accuracy can be seen as the forecasting windows are expanded, even if these improvements are not strictly monotonically increasing. However, for other sparse crimes, such as burglary, adding additional weeks of data to the forecast period does little to improve the forecast accuracy.

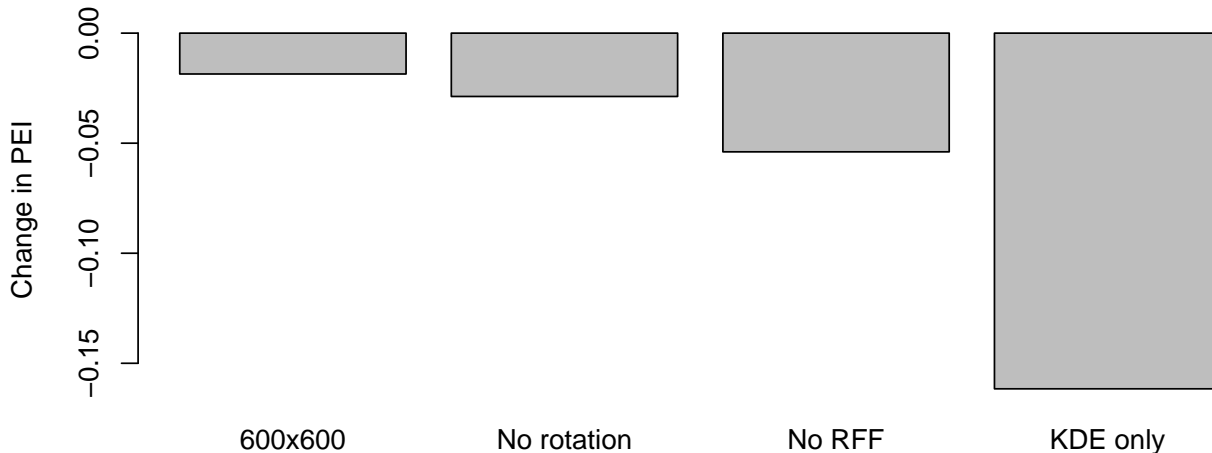


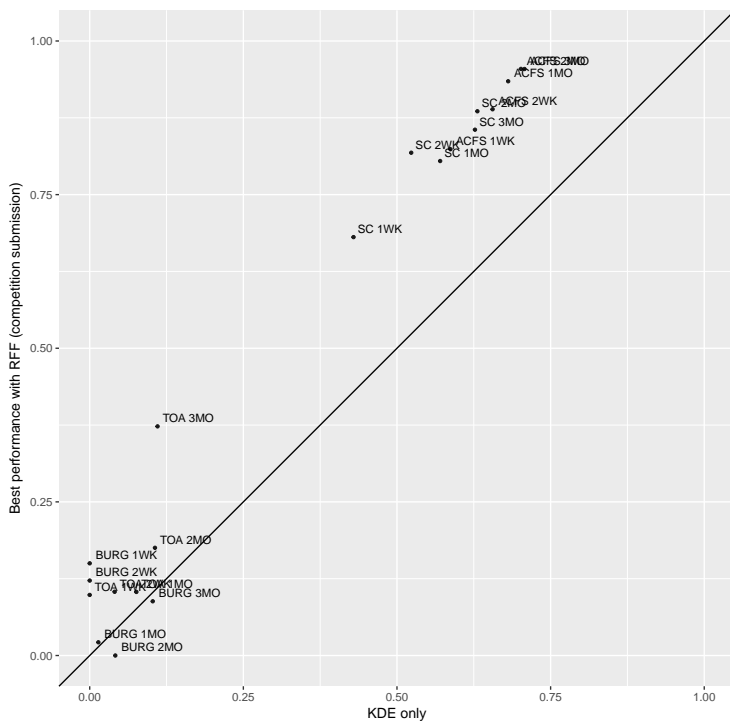
Figure 8: Comparison of various restrictions, simplifications of our model

6.2 Investigating our performance

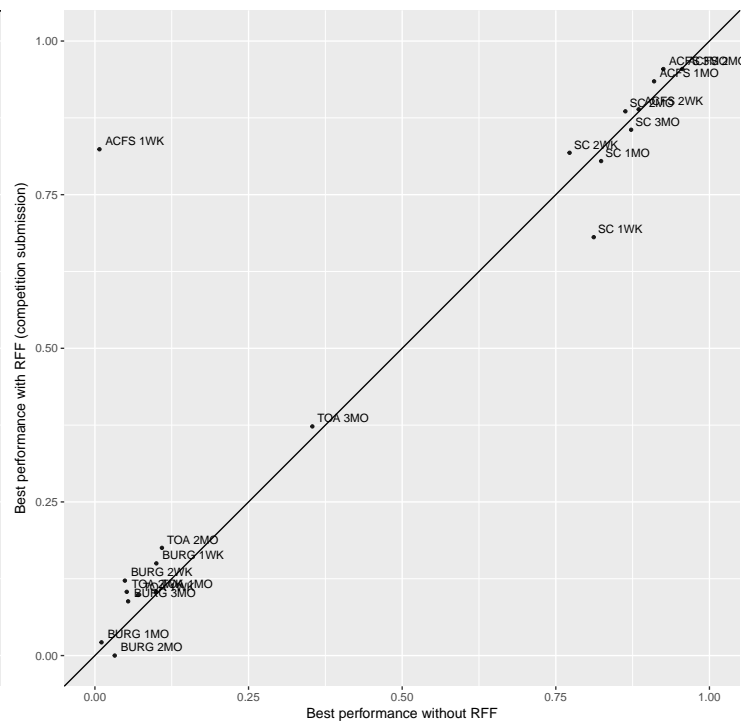
As discussed in Section 3, almost all crime forecasting in practice relies on heatmap-type approaches. As our model included lagged KDE terms, we expected to always be able to perform as well as a heatmap-type baseline. As a check, we used just one KDE lag, corresponding to a heatmap-type baseline, and fixed parameters according to common practice [Chainey and Ratcliffe, 2005] and found that our model was better than this baseline 90% of the time on the true forecasted data (March-May 2017) with an average absolute improvement of 0.16. The improvements were most notable for sparse crimes and short time-horizons, as the baseline model sometimes identified no correct vehicle or burglary hotspots (Figure 9a). Interestingly, several of the forecasts for which simple KDE outperformed our model (e.g., Burglary 2m and 3m), hyperparameters for the model were selected using Bayesian Optimization rather than grid search, suggesting that BO will not always give the optimal set of parameters.

To further investigate the importance of various parts of our model, we compared our full method, which combines lagged KDE terms and a Gaussian process surface, to a model without the Gaussian process surface (Figure 9b). Here, the full model gave better PEI results 75% of the time, with an average absolute improvement of 0.05. Thus, although our full model is still an improvement, the improvements were not as dramatic as going from a simple heatmap to our full model.

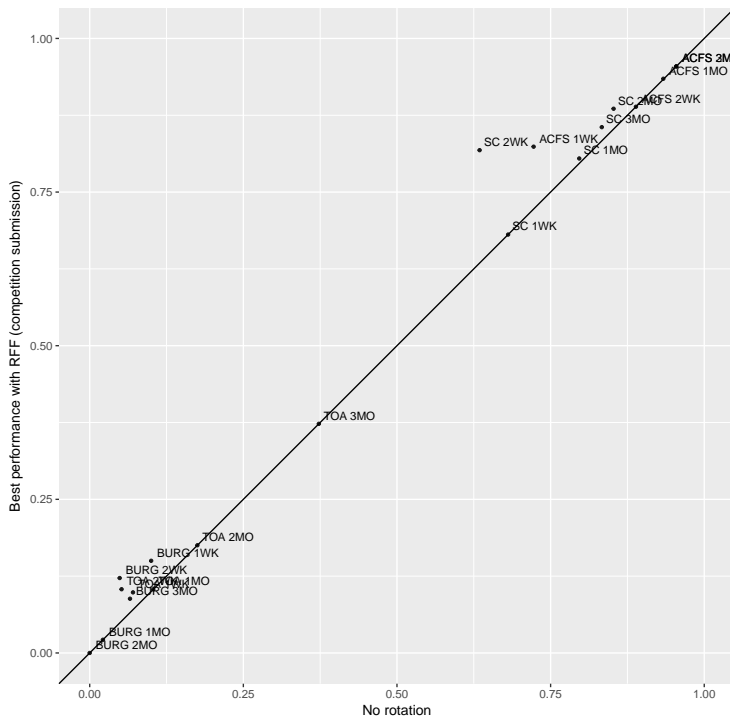
Figure 9 reports two additional comparisons. The first compares the performance of the full model to the best performing grid search model without rotation. The second compares the full model to the best performing grid search model with 600x600 sqft cells. Rosser et al. [2016] recently demonstrated that due to geocoding, non-cardinal land use, and other related factors, a non-standard alignment could improve



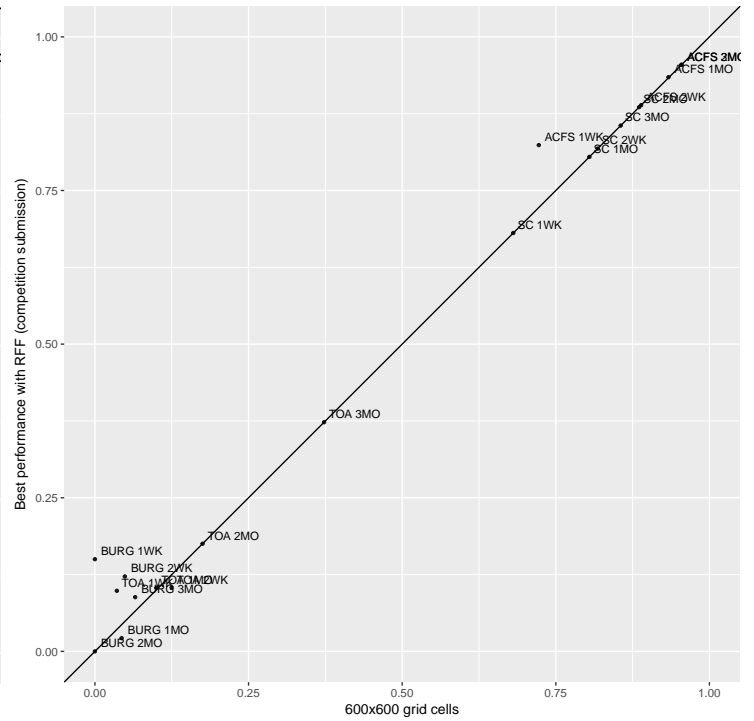
(a) KDE Baseline



(b) No random Fourier features



(c) No Rotation



(d) 600 SQFT Cells

Figure 9: Alternative Models: in each case, we compared our true competition performance (y-axis) to a restricted model (x-axis) as labeled in the caption.

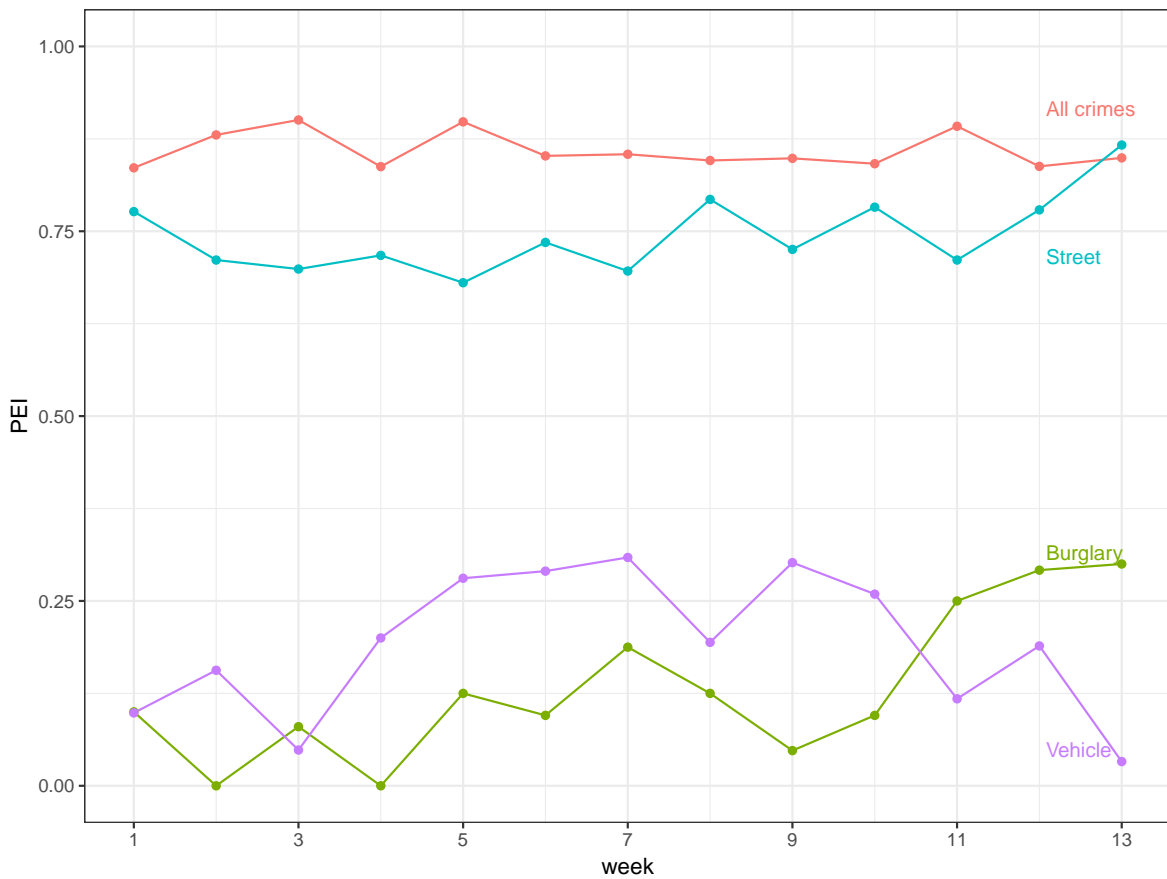


Figure 10: Rolling Forecast

predictive accuracy in crime forecasting. In the present application, we explored altering the rotation of the entire tessellation and the dimensions of the cell rectangles. With improved performance of only 0.029 for a freely-rotated model when compared to the best performing non-rotated model, rotation does not appear to be a major contributor to overall performance as can be seen in Figure 8. However, certain crime categories and forecast windows can be observed to benefit more substantially. A similar result can be observed for altering cell dimensions, which only improves overall performance by 0.019 compared to an irregular rectangle.

Since crossvalidation was used to train the model, the predictive performance achieved in test and also competition is likely to be quite stable. At the same time, the sparseness of several of the forecasted incidents and recent findings on lack of robustness of forecasting models [Rosser and Cheng, 2016] suggests that it is worthwhile to examine the repeat performance of the model. To accomplish this, the 13 week competition period (March through May 2017) was split into 13 one-week forecast periods and a one-week rolling forward prediction was made for each week. The resulting predictions, as seen in Figure 10, manifest variability consistent with the stochastic events being predicted. However, these rolling-forward predictions provide little evidence of over-fitting, even for the sparsest of incidents.

Figure 11 shows the actual performance of the full forecasting model for a high volume crime category (ACFS) and a middle-range forecasting period (1 month). Polygons that were correctly forecast as the highest

possible crime count polygons are in green. Polygons incorrectly forecast to not be hotspots are in red. And polygons that were incorrectly predicted to be the highest possible crime count polygons are depicted in blue. Crimes are black dots. As mentioned previously, the largest single cluster of hotspots for all calls for service can be seen downtown. However, the model slightly over invested in this section of Portland. As can be seen in the inset, hotspots just across the river had more crimes reported over the relevant forecast window. Most of these misses were relatively small with “false negatives” slightly “hotter” than the corresponding “false positive” cells.

Figure 12 show the actual performance of the model for a sparse crime category (burglary) and a short-range forecasting period (1 week). Forecasted burglary cells are depicted with boxes and actual burglaries are depicted by blue x’s. Boxed x’s indicate a successful prediction while empty boxes indicate a “false positive” prediction. The absence of large-scale clustering is quite visible in both the dispersion of the burglaries throughout Portland and in the similarly dispersed allocation of predictions. As can be seen in the inset, a successful prediction was accompanied by several near misses in the vicinity, including one near-miss off by only a single cell.

7 Discussion

Real-time spatiotemporal forecasting is an area of increasing interest among both practitioners and scholars. And yet, many of the approaches that are commonly in use, such as kernel-smoothing based on fixed bandwidths and cell sizes, can be quite limited in their effectiveness, even for frequent crime types but especially for sparse events. Recent work has begun exploring how sensitive forecasting accuracy is to particular parameter configurations, showing that predictive accuracy is more sensitive to bandwidth selection than cell dimensions [Chainey, 2013]. The present investigation similarly suggests that default and other rule-of-thumb parameter choices are not likely to produce the highest accuracy predictions. From a supervised learning perspective, this should come as no surprise, and so in the present study, we exhaustively tuned each of the tuning parameters in our model, showing that careful searching of commonly used parameters can produce performance improvements exceeding those achieved conventionally. Perhaps more importantly, this supervised learning exercise also revealed that while certain parameters are often more important to accuracy than others, no one parameter is universally better and as such, supervised learning across a range of parameters will likely need to be a continuing feature of spatiotemporal event forecasting.

This study also suggests the benefits of a generic framework combining two types of kernel methods—Gaussian processes and kernel smoothing. Among 9 wins in the NIJ forecasting competition, our framework performed equally well on several of the different sub-classes of the problem. Forecasting all-calls-for-service is an excellent example of a heterogeneous high volume spatiotemporal event. Other examples in this category, for which our method might be useful, include ride-sharing demand, which may be driven by a number of different use patterns. We were particularly effective at forecasting burglary, illustrating a sparse process that exhibits minimal clustering. Past work [Johnson et al., 2009] has reported 1-week burglary forecasting accuracy of 10% at 1.3% of coverage area and 25% of burglaries at 5% of coverage area using near-repeat models with baseline KDE models producing 1-week accuracy of 10% at 2% coverage and 25% at 6.5% coverage. By comparison, median 1-week burglary accuracy of 10% was achieved with a coverage area of

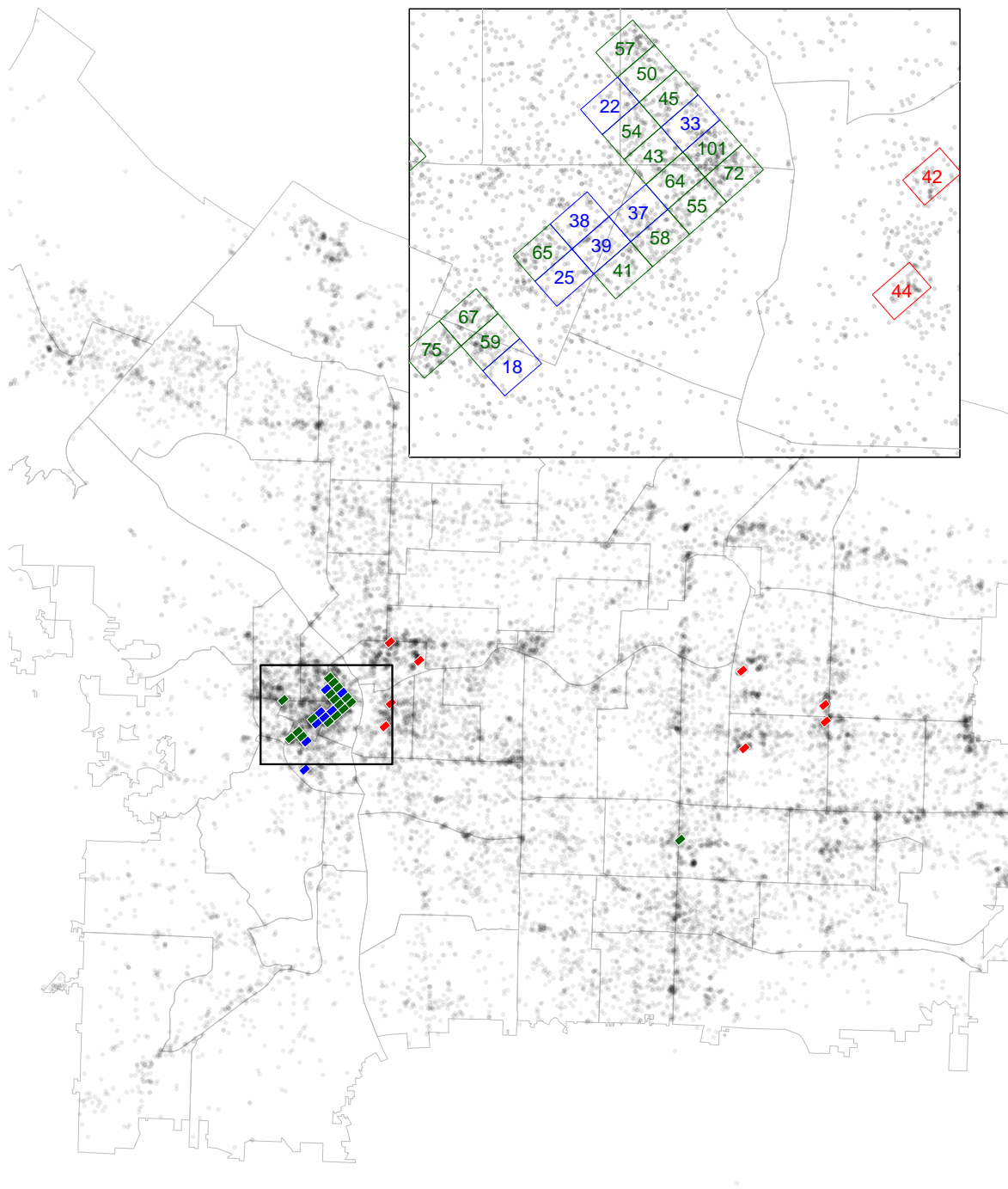


Figure 11: All Calls for Service 1 month. Correctly forecast polygons are in green. “False negative” polygons are in red. “False positive” polygons are depicted in blue. Crimes are black dots.

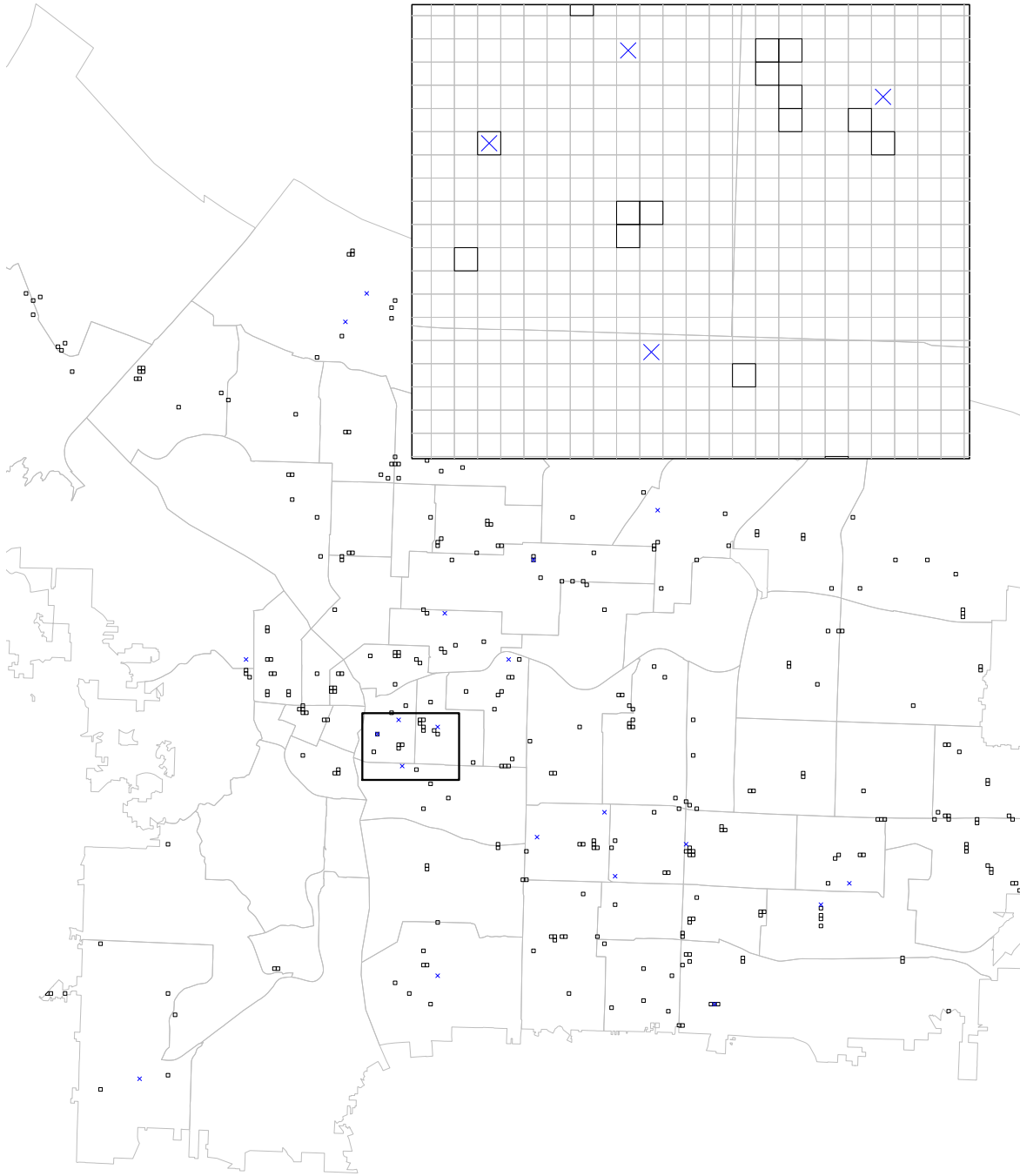


Figure 12: Burglary 1 week. Forecasted burglary cells are depicted with boxes. Actual burglaries are depicted by blue x's. Boxed x's indicate a successful prediction. Empty boxes indicate a "false positive" prediction.

0.5% and 50% of the time 25% forecasting accuracy was achieved at 0.5% coverage.¹⁴ This performance on the sparsest of forecast events over the shortest time period in the competition was sufficiently high that it not only won for the scoring metric for which it was optimized but also for the scoring metric for which it was not.

A final question to consider is what is to be done with the information generated by spatiotemporal forecasting models? In recent years, crime forecasting tools have been a supplement or replacement for traditional crime analysis, which has elevated concerns about the possible bias that could come from relying on non-randomly filtered information being the basis for deployment decisions that could lead to additional enforcement actions targeted at particular groups of individuals [Lum and Isaac, 2016]. While other possibilities beyond enforcement do exist and are actively being explored [Taniguchi and Groff, 2017], these concerns regarding the fairness implications of spatiotemporal forecasting methods are unlikely to be resolved separately from larger questions of fairness in criminal justice decision-making despite recent attempts to formulate definitions of algorithmic fairness [Corbett-Davies et al., 2017]. Whatever the eventual resolution of these concerns, bias is only one of the limitations of existing forecasting tools, the other being accuracy, which was the focus of the NIJ competition. The results reported here and elsewhere suggest that forecasting the hottest hotspots for high volume crimes can be done today with great accuracy using a range of different approaches. The same cannot be said for sparse events, at least not yet. While the accuracy of our sparse/short-term forecasts was an order of magnitude above competitors on our competition metric (PEI), it is still only in the low double-digits. This leaves as an open question, partially addressed by this paper and the NIJ competition, whether rare crime events are intrinsically harder to forecast due to random error or are simply harder because of insufficient training data. The fact that some rare crime forecasts saw no improvement in forecasting accuracy despite the addition of more data could be considered suggestive evidence that there may be a signal limit for this type of event. However, if this limit exists, it is important not to conclude it generalizes to other events, since other events or the same event in other settings may not manifest this pattern. Refitting our models in other settings, both criminological and otherwise, would shed further light on this question.

Acknowledgments

SRF was supported by EPSRC (EP/K009362/1).

¹⁴Mohler et al. [2011] report 5% accuracy for daily predictions at comparable coverage levels.

References

- Ryan Prescott Adams, Iain Murray, and David JC MacKay. Tractable nonparametric bayesian inference in poisson processes with gaussian process intensities. In *Proceedings of the 26th Annual International Conference on Machine Learning*, pages 9–16. ACM, 2009.
- Monsuru Adepeju, Gabriel Rosser, and Tao Cheng. Novel evaluation metrics for sparse spatio-temporal point process hotspot predictions - a crime case study. *International Journal of Geographical Information Science*, 30(11):2133–2154, November 2016. ISSN 1365-8816. doi: 10.1080/13658816.2016.1159684. URL <https://doi.org/10.1080/13658816.2016.1159684>.
- Mohammad Al Boni and Matthew S Gerber. Predicting crime with routine activity patterns inferred from social media. In *Systems, Man, and Cybernetics (SMC), 2016 IEEE International Conference on*, pages 001233–001238. IEEE, 2016.
- Sivan Aldor-Noiman, Lawrence D Brown, Emily B Fox, and Robert A Stine. Spatio-temporal low count processes with application to violent crime events. *arXiv preprint arXiv:1304.5642*, 2013.
- Mohammad Taha Bahadori, Qi Rose Yu, and Yan Liu. Fast multivariate spatio-temporal analysis via low rank tensor learning. In *Advances in neural information processing systems*, pages 3491–3499, 2014.
- Mohammad Al Boni and Matthew S. Gerber. Automatic optimization of localized kernel density estimation for hotspot policing. In *International Conference on Machine Learning and Applications*, pages 32–38. IEEE, December 2016. ISBN 978-1-5090-6167-9. doi: 10.1109/ICMLA.2016.0015. URL <http://ieeexplore.ieee.org/document/7838119/>.
- George EP Box, Gwilym M Jenkins, Gregory C Reinsel, and Greta M Ljung. *Time series analysis: forecasting and control*. John Wiley & Sons, 2015.
- William Bratton. *Turnaround : how America’s top cop reversed the crime epidemic /*. Random House,, New York :, 1st ed. edition, 1998. ISBN 978-0-679-45251-5.
- Leo Breiman et al. Statistical modeling: The two cultures (with comments and a rejoinder by the author). *Statistical science*, 16(3):199–231, 2001.
- Anders Brix and Peter J Diggle. Spatiotemporal prediction for log-gaussian cox processes. *Journal of the Royal Statistical Society: Series B (Statistical Methodology)*, 63(4):823–841, 2001.
- Peter J Brockwell and Richard A Davis. *Time series: theory and methods*. Springer Science & Business Media, 2013.
- Joel M. Caplan, Leslie W. Kennedy, and Joel Miller. Risk Terrain Modeling: Brokering Criminological Theory and GIS Methods for Crime Forecasting. *Justice Quarterly*, 28(2):360–381, apr 2011. doi: 10.1080/07418825.2010.486037.
- Daniel Cervone, Natesh S Pillai, Debdeep Pati, Ross Berbeco, John Henry Lewis, et al. A location-mixture autoregressive model for online forecasting of lung tumor motion. *The Annals of Applied Statistics*, 8(3): 1341–1371, 2014.

- S. P. Chainey. Examining the influence of cell size and bandwidth size on kernel density estimation crime hotspot maps for predicting spatial patterns of crime. *Bulletin of the Geographical Society of Liege*, 60: 7–19, 2013. URL <http://discovery.ucl.ac.uk/1388639/>.
- Spencer Chainey and Jerry Ratcliffe. *GIS and crime mapping*. John Wiley & Sons, 2005.
- Spencer Chainey, Lisa Tompson, and Sebastian Uhlig. Response to Levine. *Security Journal*, 21(4):303–306, sep 2008a. doi: 10.1057/sj.2008.7. URL <https://doi.org/10.10572Fsj.2008.7>.
- Spencer Chainey, Lisa Tompson, and Sebastian Uhlig. The Utility of Hotspot Mapping for Predicting Spatial Patterns of Crime. *Security Journal*, 21(1-2):4–28, January 2008b. ISSN 0955-1662, 1743-4645. doi: 10.1057/palgrave.sj.8350066. URL <http://link.springer.com/article/10.1057/palgrave.sj.8350066>.
- Taeryon Choi and Mark J Schervish. On posterior consistency in nonparametric regression problems. *Journal of Multivariate Analysis*, 98(10):1969–1987, 2007.
- Sam Corbett-Davies, Emma Pierson, Avi Feller, Sharad Goel, and Aziz Huq. Algorithmic decision making and the cost of fairness. *arXiv preprint arXiv:1701.08230*, 2017.
- N. Cressie and C.K. Wikle. *Statistics for spatio-temporal data*, volume 465. Wiley, 2011.
- N. A. C. Cressie. *Statistics for spatial data*. Wiley Series in Probability and Mathematical Statistics: Applied Probability and Statistics. John Wiley & Sons Inc., New York, 1993. ISBN 0-471-00255-0.
- John P Cunningham, Krishna V Shenoy, and Maneesh Sahani. Fast gaussian process methods for point process intensity estimation. In *Proceedings of the 25th international conference on Machine learning*, pages 192–199. ACM, 2008.
- Peter J Diggle. *Statistical analysis of spatial and spatio-temporal point patterns*. CRC Press, 2013.
- Peter J Diggle, Paula Moraga, Barry Rowlingson, Benjamin M Taylor, et al. Spatial and spatio-temporal log-gaussian cox processes: extending the geostatistical paradigm. *Statistical Science*, 28(4):542–563, 2013.
- T. Fernandez and Y. W. Teh. Posterior consistency for a non-parametric survival model under a Gaussian process prior. ArXiv e-prints: 1611.02335, 2016.
- Seth Flaxman, Andrew Wilson, Daniel Neill, Hannes Nickisch, and Alex Smola. Fast kronecker inference in gaussian processes with non-gaussian likelihoods. In *International Conference on Machine Learning*, pages 607–616, 2015.
- Seth R Flaxman. A general approach to prediction and forecasting crime rates with gaussian processes. *Heinz College Technical Report*, 2014. URL https://www.ml.cmu.edu/research/dap-papers/dap_flaxman.pdf.
- Kyle J Foreman, Guangquan Li, Nicky Best, and Majid Ezzati. Small area forecasts of cause-specific mortality: application of a bayesian hierarchical model to us vital registration data. *Journal of the Royal Statistical Society: Series C (Applied Statistics)*, 66(1):121–139, 2017.
- Matthew S Gerber. Predicting crime using twitter and kernel density estimation. *Decision Support Systems*, 61:115–125, 2014.

- E. Gilboa, Y. Saatci, and J. Cunningham. Scaling multidimensional inference for structured gaussian processes. *Pattern Analysis and Machine Intelligence, IEEE Transactions on*, PP(99):1–1, 2013. ISSN 0162-8828. doi: 10.1109/TPAMI.2013.192.
- Georg M Goerg and Cosma Rohilla Shalizi. Licors: Light cone reconstruction of states for non-parametric forecasting of spatio-temporal systems. *arXiv preprint arXiv:1206.2398*, 2012.
- Wilpen Gorr, Andreas Olligschlaeger, and Yvonne Thompson. Short-term forecasting of crime. *International Journal of Forecasting*, 19(4):579–594, oct 2003. ISSN 0169-2070. doi: 10.1016/S0169-2070(03)00092-X. URL <http://www.sciencedirect.com/science/article/pii/S016920700300092X>.
- Wilpen L Gorr. Forecast accuracy measures for exception reporting using receiver operating characteristic curves. *International Journal of Forecasting*, 25(1):48–61, 2009.
- Wilpen L. Gorr and YongJei Lee. Early Warning System for Temporary Crime Hot Spots. *Journal of Quantitative Criminology*, 31(1):25–47, March 2015. ISSN 0748-4518, 1573-7799. doi: 10.1007/s10940-014-9223-8. URL <http://link.springer.com/article/10.1007/s10940-014-9223-8>.
- Timothy Hart and Paul Zandbergen. Kernel density estimation and hotspot mapping: Examining the influence of interpolation method, grid cell size, and bandwidth on crime forecasting. *Policing: An International Journal of Police Strategies & Management*, 37(2):305–323, May 2014. ISSN 1363-951X. doi: 10.1108/PIJPSM-04-2013-0039. URL <http://www.emeraldinsight.com/doi/full/10.1108/PIJPSM-04-2013-0039>.
- Philipp Hennig, Michael A. Osborne, and Mark Girolami. Probabilistic numerics and uncertainty in computations. *Proceedings of the Royal Society of London A: Mathematical, Physical and Engineering Sciences*, 471(2179), 2015.
- Amanda S Hering and Marc G Genton. Powering up with space-time wind forecasting. *Journal of the American Statistical Association*, 105(489):92–104, 2010.
- Hsin-Cheng Huang and Noel Cressie. Spatio-temporal prediction of snow water equivalent using the kalman filter. *Computational Statistics & Data Analysis*, 22(2):159–175, 1996.
- Joel M Hunt. *Do crime hot spots move? Exploring the effects of the modifiable areal unit problem and modifiable temporal unit problem on crime hot spot stability*. PhD thesis, American University, 2016.
- Shane D Johnson, Kate J Bowers, D.J. Birks, and Ken Pease. Predictive mapping of crime by ProMap: accuracy, units of analysis, and the environmental backcloth. In David Weisburd, Wim Bernasco, and Gerben Bruinsma, editors, *Putting Crime in its Place*, pages 165–192. Springer, Dordrecht, 2009.
- Hyeon-Woo Kang and Hang-Bong Kang. Prediction of crime occurrence from multi-modal data using deep learning. *PLOS ONE*, 12(4):e0176244, apr 2017. doi: 10.1371/journal.pone.0176244. URL <https://doi.org/10.13712Fjournal.pone.0176244>.
- Leslie W Kennedy, Joel M Caplan, and Eric Piza. Risk clusters, hotspots, and spatial intelligence: risk terrain modeling as an algorithm for police resource allocation strategies. *Journal of Quantitative Criminology*, 27(3):339–362, 2011.

- S. Lavigne, B. Clifton, and F. Tseng. Predicting Financial Crime: Augmenting the Predictive Policing Arsenal. *ArXiv e-prints*, April 2017.
- Ned Levine. CrimeStat: a spatial statistics program for the analysis of crime incident locations, version 3.0. Technical report, Ned Levine and Associates/National Institute of Justice, Washington, DC, 2004.
- Erik Lewis, George Mohler, P Jeffrey Brantingham, and Andrea L Bertozzi. Self-exciting point process models of civilian deaths in Iraq. *Security Journal*, 25(3):244–264, sep 2011. doi: 10.1057/sj.2011.21. URL <https://doi.org/10.10572Fsj.2011.21>.
- Hua Liu and Donald E. Brown. Criminal incident prediction using a point-pattern-based density model. *International Journal of Forecasting*, 19(4):603–622, Oct 2003. ISSN 0169-2070. doi: 10.1016/S0169-2070(03)00094-3. URL <http://www.sciencedirect.com/science/article/pii/S0169207003000943>.
- Chris Lloyd, Tom Gunter, Michael Osborne, and Stephen Roberts. Variational inference for gaussian process modulated poisson processes. In *International Conference on Machine Learning*, pages 1814–1822, 2015.
- Charles Loeffler and Seth Flaxman. Is gun violence contagious? *Journal of Quantitative Criminology*, 2017. URL <https://arxiv.org/abs/1611.06713>.
- Kristian Lum and William Isaac. To predict and serve? *Significance*, 13(5):14–19, 2016.
- Russell L Martin and JE Oeppen. The identification of regional forecasting models using space: time correlation functions. *Transactions of the Institute of British Geographers*, pages 95–118, 1975.
- G. O. Mohler, M. B. Short, P. J. Brantingham, F. P. Schoenberg, and G. E. Tita. Self-Exciting Point Process Modeling of Crime. *Journal of the American Statistical Association*, 106(493):100–108, mar 2011. doi: 10.1198/jasa.2011.ap09546. URL <https://doi.org/10.11982Fjasa.2011.ap09546>.
- George Mohler. Marked point process hotspot maps for homicide and gun crime prediction in chicago. *International Journal of Forecasting*, 30(3):491–497, 2014.
- George Mohler and Michael D. Porter. Rotational grid, pai-maximizing crime forecasts. 2017.
- Jesper Møller and Jakob G Rasmussen. Perfect simulation of hawkes processes. *Advances in applied probability*, 37(3):629–646, 2005.
- Jesper Møller, Anne Randi Syversveen, and Rasmus Plenge Waagepetersen. Log gaussian cox processes. *Scandinavian journal of statistics*, 25(3):451–482, 1998.
- George D Montañez and Cosma Rohilla Shalizi. The licors cabinet: Nonparametric light cone methods for spatio-temporal modeling. In *Neural Networks (IJCNN), 2017 International Joint Conference on*, pages 2811–2819. IEEE, 2017.
- NIJ. Real-Time Crime Forecasting Challenge, 2017. URL <http://www.nij.gov:80/funding/Pages/fy16-crime-forecasting-challenge.aspx>.
- Yosihiko Ogata. Statistical models for earthquake occurrences and residual analysis for point processes. *Journal of the American Statistical association*, 83(401):9–27, 1988.

- Anthony O’Hagan. Some bayesian numerical analysis. *Bayesian Statistics*, 4(345–363):4–2, 1992.
- Kenneth Pease et al. *Repeat victimisation: Taking stock*, volume 90. Home Office Police Research Group London, 1998.
- Walter L. Perry, Brian McInnis, Carter C. Price, Susan C. Smith, and John S. Hollywood. Predictive Policing: The Role of Crime Forecasting in Law Enforcement Operations. Technical report, RAND Corporation, Santa Monica, 2013.
- Michael D. Porter and Brian J. Reich. Evaluating temporally weighted kernel density methods for predicting the next event location in a series. *Annals of GIS*, 18(3):225–240, September 2012. ISSN 1947-5683. doi: 10.1080/19475683.2012.691904. URL <https://doi.org/10.1080/19475683.2012.691904>.
- Joaquin Quiñonero Candela, Carl Edward Rasmussen, Aníbal R Figueiras-Vidal, et al. Sparse spectrum gaussian process regression. *Journal of Machine Learning Research*, 11(Jun):1865–1881, 2010.
- Ali Rahimi and Benjamin Recht. Random features for large-scale kernel machines. In *Advances in neural information processing systems*, pages 1177–1184, 2007.
- Ali Rahimi and Benjamin Recht. Weighted sums of random kitchen sinks: Replacing minimization with randomization in learning. In *Advances in neural information processing systems*, pages 1313–1320, 2008.
- Carl Edward Rasmussen and Christopher KI Williams. *Gaussian processes for machine learning*, 2006.
- Brian D. Ripley. *Spatial Statistics*. Wiley, New York, 1981.
- Gabriel Rosser and Tao Cheng. Improving the robustness and accuracy of crime prediction with the self-exciting point process through isotropic triggering. *Applied Spatial Analysis and Policy*, pages 1–21, 2016.
- Gabriel Rosser, Toby Davies, Kate J. Bowers, Shane D. Johnson, and Tao Cheng. Predictive crime mapping: Arbitrary grids or street networks? *Journal of Quantitative Criminology*, pages 1–26, sep 2016. ISSN 0748-4518, 1573-7799. doi: 10.1007/s10940-016-9321-x. URL <http://link.springer.com/article/10.1007/s10940-016-9321-x>.
- Yunus Saatçi. *Scalable inference for structured Gaussian process models*. PhD thesis, University of Cambridge, 2011.
- Sujit Kumar Sahu and Khandoker Shuvo Bakar. Hierarchical bayesian autoregressive models for large space–time data with applications to ozone concentration modelling. *Applied Stochastic Models in Business and Industry*, 28(5):395–415, 2012.
- Bernhard Schölkopf and Alexander J Smola. *Learning with kernels: support vector machines, regularization, optimization and beyond*. the MIT Press, 2002.
- Harold G. Schutt. Advanced police methods in berkeley. *National Municipal Review*, 11(3):80–85, 1922. ISSN 1931-0250. doi: 10.1002/ncr.4110110308. URL <http://dx.doi.org/10.1002/ncr.4110110308>.
- Galit Shmueli et al. To explain or to predict? *Statistical science*, 25(3):289–310, 2010.

- Edward Snelson and Zoubin Ghahramani. Sparse gaussian processes using pseudo-inputs. In *Advances in neural information processing systems*, pages 1257–1264, 2006.
- Jasper Snoek, Hugo Larochelle, and Ryan P Adams. Practical bayesian optimization of machine learning algorithms. In *Advances in neural information processing systems*, pages 2951–2959, 2012.
- Michael L Stein. *Interpolation of Spatial Data: Some Theory for Kriging*. Springer Science & Business Media, 1999.
- Jonathan R Stroud, Peter Müller, and Bruno Sansó. Dynamic models for spatiotemporal data. *Journal of the Royal Statistical Society: Series B (Statistical Methodology)*, 63(4):673–689, 2001.
- Matthew A. Taddy. Autoregressive Mixture Models for Dynamic Spatial Poisson Processes: Application to Tracking Intensity of Violent Crime. *Journal of the American Statistical Association*, 105(492):1403–1417, December 2010. ISSN 0162-1459. doi: 10.1198/jasa.2010.ap09655. URL <http://dx.doi.org/10.1198/jasa.2010.ap09655>.
- Travis Taniguchi and Elizabeth R. Groff. Near Repeat Burglary Intervention, 2017. URL <https://www.policefoundation.org/projects/near-repeat-burglary-intervention/>.
- Yee W Teh and Vinayak Rao. Gaussian process modulated renewal processes. In *Advances in Neural Information Processing Systems*, pages 2474–2482, 2011.
- Michalis Titsias. Variational learning of inducing variables in sparse gaussian processes. In *Artificial Intelligence and Statistics*, pages 567–574, 2009.
- Waldo R Tobler. A computer movie simulating urban growth in the detroit region. *Economic geography*, pages 234–240, 1970.
- Stefano F Tonellato. Spatial prediction with space-time models. In *Between Data Science and Applied Data Analysis*, pages 358–366. Springer, 2003.
- Xiaofeng Wang, Matthew S. Gerber, and Donald E. Brown. Automatic Crime Prediction Using Events Extracted from Twitter Posts. In *Social Computing Behavioral - Cultural Modeling and Prediction*, pages 231–238. Springer Berlin Heidelberg, 2012.
- Christopher K Wikle, L Mark Berliner, and Noel Cressie. Hierarchical bayesian space-time models. *Environmental and Ecological Statistics*, 5(2):117–154, 1998.
- Christopher KI Williams and Matthias Seeger. Using the nyström method to speed up kernel machines. In *Advances in neural information processing systems*, pages 682–688, 2001.
- Andrew G Wilson and Ryan P Adams. Gaussian process kernels for pattern discovery and extrapolation. In *ICML*, pages 1067–1075, 2013.
- Andrew Gordon Wilson, Elad Gilboa, Arye Nehorai, and John P. Cunningham. Fast kernel learning for multidimensional pattern extrapolation. In *Advances in Neural Information Processing Systems*. MIT Press, 2014. URL <http://www.cs.cmu.edu/~andrewgw/manet.pdf>.

- Yuanfu Xie, S Koch, J McGinley, S Albers, PE Bieringer, M Wolfson, and M Chan. A space–time multiscale analysis system: A sequential variational analysis approach. *Monthly Weather Review*, 139(4):1224–1240, 2011.
- A. Zammit-Mangion, M. Dewar, V. Kadiramanathan, and G. Sanguinetti. Point process modelling of the Afghan War Diary. *Proceedings of the National Academy of Sciences*, 109(31):12414–12419, jul 2012. doi: 10.1073/pnas.1203177109. URL <https://doi.org/10.10732Fpnas.1203177109>.
- Hui Zou and Trevor Hastie. Regularization and variable selection via the elastic net. *Journal of the Royal Statistical Society: Series B (Statistical Methodology)*, 67(2):301–320, 2005.

A Appendix

A.1 Hyperparameter choice

delx	dely	alpha	eta	lt	theta	k	l1	l2	kde.bw	kde.lags	kde.win	crime	period
478	710	0.10	2.28	67.10	0.85	362	0	5e-5	274.70	9	39.62	all	1m
618	473	0.16	1.83	42.93	0.25	360	0	0	391.97	9	68.73	all	1w
600	600	0	1	60	0	250	0	1e-5	500	8	45	all	2m
600	600	0	1	28	0	250	0	5e-4	500	12	45	all	2w
600	600	0.05	2	90	0	20	1e-5	1e-4	500	6	90	all	3m
250	250	0.95	0.50	60	0	5	0	5e-5	250	12	15	burglary	1m
250	250	0.95	3	7	0	20	0	0	250	6	10	burglary	1w
431	598	0.10	5	18.95	0	10	0	1e-4	342.42	10	3.50	burglary	2m
250	250	1	0.50	70	0	5	0	1e-5	250	6	21	burglary	2w
689	484	0.15	3.39	105.96	0.37	36	0	0	597.12	4	14.77	burglary	3m
600	600	0.15	2	15	0.98	20	0	0	500	3	15	street	1m
600	600	0.10	0.50	3.50	0	250	0	0	500	6	7	street	1w
600	600	0.10	1.50	120	0.98	20	0	0	500	1	60	street	2m
600	600	0.05	0.50	7	0.98	250	0	0	500	3	14	street	2w
600	600	0	2	90	1.18	20	0	5e-4	500	3	45	street	3m
800	450	0	0.50	150	0	5	0	5e-4	500	3	15	vehicle	1m
250	250	0.95	2	49	0	5	0	0	250	6	10	vehicle	1w
600	600	0.80	0.50	60	0	20	0	0	500	1	30	vehicle	2m
250	250	1	3	14	0	5	0	0	250	3	21	vehicle	2w
600	600	0	0.50	180	0	20	0	1e-5	500	3	45	vehicle	3m

Table A1: Hyperparameters we selected. Yellow are winning rows. We also won for the PAI metric for burglary 1 week and 2 week.